



Toward an estimation of global land surface heat fluxes from multisatellite observations

Carlos Jiménez,¹ Catherine Prigent,¹ and Filipe Aires²

Received 31 October 2008; revised 14 January 2009; accepted 28 January 2009; published 31 March 2009.

[1] The sensitivity of a suite of satellite observations to land surface heat fluxes and the estimation of satellite-derived fluxes using a statistical model are investigated. The satellite data include visible and near-infrared reflectances (Advanced Very High Resolution Radiometer [AVHRR]), thermal infrared surface skin temperature and its diurnal cycle (International Satellite Cloud Climatology Project [ISCCP]), active microwave backscatter (European Remote-sensing Satellite [ERS] scatterometer), and passive microwave emissivities (Special Sensor Microwave/Imager [SSM/I]). Fluxes at the global scale are taken from Land Surface Models (LSM): the GSWP-2 multimodel analysis, the ISBA, and ORCHIDEE participating models, along with the National Centers for Environmental Prediction/the National Center for Atmospheric Research (NCEP/NCAR) reanalysis, on a monthly timescale from 1993 to 1995. The simulated LSM fluxes and the satellite observations are linked through a statistical model. Once calibrated, the statistical model reproduces the LSM latent and sensible fluxes for all types of snow-free environments, with global RMS errors $<25 \text{ W/m}^2$, proving that the satellite data contain relevant information for flux estimation. The estimated fluxes have realistic spatial and seasonal patterns, although some local differences between the original and estimated fluxes are found. These differences are used to reveal potential problems in the LSMs, for instance, an anomaly in the GSWP-2 radiative forcings. Comparisons between the original and estimated fluxes and 76 tower fluxes over North America are carried out, and the differences show similar statistics. However, the largest differences between the original and estimated fluxes do not occur in these regions. Demonstrating the superiority of the proposed technique outside of these regions remains difficult in the absence of validation data sets.

Citation: Jiménez, C., C. Prigent, and F. Aires (2009), Toward an estimation of global land surface heat fluxes from multisatellite observations, *J. Geophys. Res.*, 114, D06305, doi:10.1029/2008JD011392.

1. Introduction

[2] Land surface heat fluxes are essential components of the water and energy cycles and govern the interactions between the Earth surface and the atmosphere [e.g., *Betts et al.*, 1996]. Variables such as cloud cover, precipitation, surface radiation, or air temperature and humidity, which are related to the atmospheric synoptic patterns and meso-scale structures, strongly influence the heat fluxes. In turn, the energy balance at the surface and its partitioning between sensible and latent heat fluxes also affect the atmosphere, determining the development of the atmospheric boundary layer [e.g., *Viterbo and Beljaars*, 1995]. Over land, energy balance and flux partitioning are complex

mechanisms, with strong variabilities in both space and time, across climates and ecosystems, related to the physical properties of the surface, especially its moisture status and vegetation. In situ measurements of land surface heat fluxes are operated during field experiments (e.g., the Boreal Ecosystem-Atmosphere Study (BOREAS) [*Sellers et al.*, 1997]) and by some flux tower networks (e.g., FLUXNET [*Baldocchi et al.*, 2001]), but in order to obtain global, consistent estimates of the surface heat fluxes, a transition to satellite remote sensing is needed. The challenge is that fluxes do not have a unique signature that can be remotely and directly detected, and satellite observations related to surface temperature, soil moisture, or vegetation have to be combined to infer the fluxes.

[3] In principle bulk transfer calculations from the aerodynamic theory of turbulent transfer [e.g., *Tarpley*, 1994] can produce fluxes. Using these formulations and a satellite surface-derived skin temperature T_{ss} as a proxy for the aerodynamic surface temperature T_{as} , the sensible heat flux can be derived from the difference between the skin temperature T_{ss} and a measured air temperature T_a , scaled by a transfer coefficient characterizing the transport of heat

¹Laboratoire d'Etudes du Rayonnement et de la Matière en Astrophysique, Centre National de la Recherche Scientifique, Observatoire de Paris, Paris, France.

²Laboratoire de Météorologie Dynamique, Institut Pierre-Simon Laplace/Centre National de la Recherche Scientifique, Université Pierre et Marie Curie, Paris, France.

and depending on site-specific data, such as surface roughness or wind speed. The latent heat flux can then be estimated from an energy balance model, assuming the surface radiation and the ground flux are known. Difficulties first arise from the fact that differences between T_{ss} and T_a are rather limited and the accuracy of each measurement (often of the same order of their difference) can have a detrimental effect on the estimated sensible heat flux. In addition, the difference between T_{as} and T_{ss} can be significant [e.g., *Kustas and Humes*, 1997], as well as the difference between the soil and the vegetation temperatures with only one integrated temperature being estimated from satellite [e.g., *Norman et al.*, 1995; *Kustas and Norman*, 2000; *Nishida et al.*, 2003]. Still on the basis of the bulk formulation, more elaborated models try to overcome some of these difficulties by exploiting the relationship between soil moisture and thermal inertia, with formulations to constrain the heat fluxes with the diurnal gradient of T_{ss} [e.g., *Tarpley*, 1994; *Meng et al.*, 2003; *Mecikalski et al.*, 1999; *Anderson et al.*, 2007, *Caparrini et al.*, 2004]. Other schemes use relationships between T_{ss} and other satellite observations, such as the vegetation index [e.g., *Carlson et al.*, 1995; *Nishida et al.*, 2003]. In general, these approaches require large amounts of ancillary data that are globally not easily accessible (such as surface roughness or surface meteorological data), making difficult a possible extension to estimating global heat fluxes.

[4] The only source of realistic land surface heat fluxes available today, with the adequate time and space samplings, are calculated from complex land surface models (LSMs). However, inter-comparisons of the LSM outputs show very large differences, due to model parameterizations and forcings (e.g., the Project to Intercompare Land-Surface Parameterization Schemes (PILPS) [*Henderson-Sellers et al.*, 1995] and the Global Soil Wetness Project (GSWP) version 1 and 2 [*Entin et al.*, 1999; *Dirmeyer et al.*, 2006]). Parameterizations are often developed empirically and tuned to local conditions where the ancillary data needed to estimate the model parameters are measured [e.g., *Wilson et al.*, 2002; *Wright et al.*, 1995]. Some parameters, such as fractional vegetation cover or leaf area index, can be estimated from satellites, but many other parameters are derived from approximate relationships with vegetation, soil type, or climate regime. Complex multicriteria and multi-objective calibration schemes are developed to evaluate the parameterizations [e.g., *Franks and Beven*, 1997; *Gupta et al.*, 1998], but they can only be tested at field scales with in situ measured fluxes and local meteorological data [e.g., *Franks et al.*, 1999; *Gupta et al.*, 1999]. Efforts to use remotely sensed data in multiobjective calibration have started, but mostly limited to incorporating radiometric skin temperatures [e.g., *Crow et al.*, 2003; *Coudert et al.*, 2006]. Assimilation schemes are also used. For instance, the Global Land Data Assimilation System (GLDAS) [*Rodell et al.*, 2004] assimilates 6 hourly skin temperature observations.

[5] Despite all this body of work, there is no systematic satellite data analysis underway to produce a complete, physically consistent, global, multidecadal land surface heat flux data product. The Global Energy and Water Cycle Experiment (GEWEX) Radiation Panel (GRP) recently launched an activity, called LANDFLUX, to develop the

needed capabilities to produce such data sets. The challenge is to transition from the local or regional scales, where most previous approaches have been tested, to the global scale. Satellite observations provide the needed global coverage, but their use is difficult. For instance, traditional methods to directly assimilate satellite observations require radiative transfer models: such models do not exist globally for most flux-sensitive satellite observations such as passive or active microwaves. Another approach is the assimilation in the LSM of pre-derived satellite parameters such as soil moisture, but this is also problematic: the accuracy of such products is still questionable [e.g., *Cashion et al.*, 2005; *Zhang et al.*, 2008]. Faced with these difficulties, this study proposes to link global satellite observations with land surface heat fluxes by means of a statistical model. Contrarily to the techniques previously described, the relationship between the satellite data and the land surface heat fluxes is not prescribed, but derived from the statistical analysis of a global data set of coincident satellite observations and land surface heat fluxes. To avoid any conclusions biased by the selection of a specific model, several LSMs are tested in this study, including dedicated land surface schemes and one coupled land-atmosphere model from a meteorological operational center.

[6] The proposed statistical model mixes in a complex way the satellite observations and the LSM fluxes. In this regard, it can be considered as an assimilation technique that combines observations and model estimates, as suggested in the study by *Aires et al.* [2005] and *Aires and Prigent* [2006]. As with any assimilation technique, there is a need to test that the assimilated fields are closer to the true fields than the original fields. This is specially challenging when dealing with land surface heat fluxes, as the data needed for the evaluations is extremely limited. Faced with these limitations, the objective of the paper is to show the potential of the statistical modeling to advance in the estimation of global land surface heat fluxes, rather than to show the absolute superiority of this technique with respect to other flux estimation methods. Firstly, the statistical model is used to assess the information content of the satellite observations (some of them not used before for the estimation of fluxes), using a similar approach as in the study by *Aires et al.* [2005]. Secondly, the statistical model is used to check the consistency between the time evolution or the geographical distribution of the LSM fluxes and the satellite observations, and to potentially diagnose specific problems in the LSMs. While the LSM and statistical model fluxes will have similar global biases, discrepancies at specific regions and periods can be useful for identifying errors and anomalous behavior. A related methodology has been adopted at a local scale in the study by *Abramowitz* [2005]: a statistical model linking meteorological forcings and in situ heat fluxes helps assess the ability of the LSMs to reproduce the time evolution of the fluxes at three field sites. At the global scale, a statistical model, similar to the model proposed here but linking satellite observations and global soil moisture, proved successful in detecting inconsistencies in the soil wetness fields calculated by the National Centers for Environmental Prediction/the National Center for Atmospheric Research (NCEP/NCAR) reanalysis [*Aires et al.*, 2005].

[7] In this study, a range of model-derived global flux data sets and satellite products are selected. Flux outputs from the GSWP exercise are chosen, along with fluxes calculated by the NCEP/NCAR atmospheric reanalysis. A 3-year period (1993–1995) at a monthly scale is chosen for the study, as this is the more recent period of the GSWP exercise. Satellite observations are selected on the basis of their sensitivity to state variables (e.g., surface skin temperature and moisture) physically related to the fluxes, their availability over the globe with spatial resolutions compatible with climate analysis, and their temporal coverage of at least a decade. The selection includes thermal infrared land skin temperatures compiled by the International Satellite Cloud Climatology Project (ISCCP), the amplitude of their diurnal cycle, microwave emissivities from the Special Sensor Microwave/Imager (SSM/I), microwave radar backscattering coefficients from the European Remote-sensing Satellite (ERS), visible and near-infrared reflectances from the Advanced Very High Resolution Radiometer (AVHRR), and a surface radiation product based on the ISCCP data sets. First, the statistical model and its calibration is presented in section 2. The satellite observations and global fluxes are described in section 3. An evaluation of the sensitivity of the satellite observations to the land fluxes is presented in section 4. The capability of the statistical model to reproduce the time and spatial patterns of the fluxes is investigated in section 5, including a comparison of original and estimated fluxes with in situ tower flux measurements. Section 6 concludes this study.

2. Statistical Model

[8] Using a statistical approach to study the relationship between satellite data and heat fluxes is not new. In the study by Wang *et al.* [2007], the correlations between in situ measurements of latent heat fluxes and the net radiation, air or radiometric surface skin temperature, and vegetation indices, are tested at different field sites, and a statistical model based on a simple linear regression is proposed to estimate the latent fluxes. The scheme is applied at regional scale, where a linear mapping between the satellite observations and the fluxes is considered to be a reasonable approximation, given that the environment variables (e.g., soil moisture, vegetation, temperature) are not significantly different. At a global scale, more complex relations are expected between the land surface heat fluxes and the satellite measurements. As a consequence, a more sophisticated statistical model, a neural network (NN), is adopted in this study. The capability of representing complex non-linear mappings between multidimensional spaces makes the NNs to be broadly used for modeling non-linear processes [e.g., Aires *et al.*, 2001; Krasnopolski, 2007]. In fact, a NN scheme has already been tested to estimate latent heat flux from satellite observations [Bourras *et al.*, 2002] but over ocean, and a NN algorithm proved useful to correct for systematic errors between field observations and modeled heat fluxes at local scales [Abramowitz *et al.*, 2006, 2007].

[9] Setting up the statistical model involves different phases. In our study, in a first phase, the NN is trained to retrieve the reference LSM outputs, called here the “original fluxes”, from the satellite observations. This is the calibra-

tion phase of the statistical model. Note that for each LSM, a specific statistical model is calibrated with the fluxes from that LSM. In statistical terms, this phase corresponds to training the NN to approximate the posterior distribution of the fluxes conditioned on the satellite data. In a second phase, the trained NNs are used to produce flux estimates, called here the “estimated fluxes”, from the corresponding satellite observations. The estimated fluxes are the mean states of the previous distribution for each realization of the satellite observations presented at the NN inputs. In a third phase, the estimated fluxes are evaluated by comparison with the original fluxes and other sources of independent fluxes, when they exist. The three phases are illustrated in Figure 1.

[10] The practical details of the statistical model follow. Multilayer perceptrons (MLPs) are the NN architecture selected here. For each LSM there is a MLP trained to reproduce the fluxes from that specific model. Each MLP has as many input nodes as the number of satellite products used in the estimation. Then there is one hidden layer consisting of a number of neurons with hyperbolic tangent activation functions, followed by two output neurons with a linear activation function, one for the sensible fluxes, the second one for the latent fluxes. The weights of the MLP are initialized following the method by Nguyen and Widrow [1990], and before training inputs and outputs to the MLP are linearly transformed into the range $[-1,1]$ to make the initialization of the weights more effective. The weights are estimated by minimizing a cost function following the implementation of Foresee and Hagan [1997]. This results in MLPs with good generalization and the adequate model complexity.

[11] The training data set is built with data from the months of February, May, August, and November 1993. For these months the total number of pixels is randomly divided into two subsets of equal size: one is attached to the training data set, the other is saved to estimate the error fluxes for these months. Tests have been conducted with different training data sets (more months in a given season), but the results were very similar, indicating that one month per season is sufficient to capture the annual variability. No data from the remaining two years have been included in the training, in order to show that the statistical model driven by the satellite observations can capture the flux inter-annual variability.

3. Data Sources

[12] The satellite observations and the model-derived fluxes are re-gridded into a common global equal area grid ($0.25^\circ \times 0.25^\circ$ at the equator, with a pixel area of approximately 770 km^2) and averaged into monthly means. Shorter timescales are possible, but for a first evaluation of sensitivities this time resolution is adequate and in line with the objective of deriving a global multidecadal monthly mean climatology. For this initial study, only snow-free pixels are kept (using the National Snow and Ice Data Center (NSIDC) monthly mean snow data set), as the interpretation of some of the satellite observations and modeled fluxes over snow areas can be problematic. Examples of monthly mean satellite observations for June 1993 are given in Figure 2.

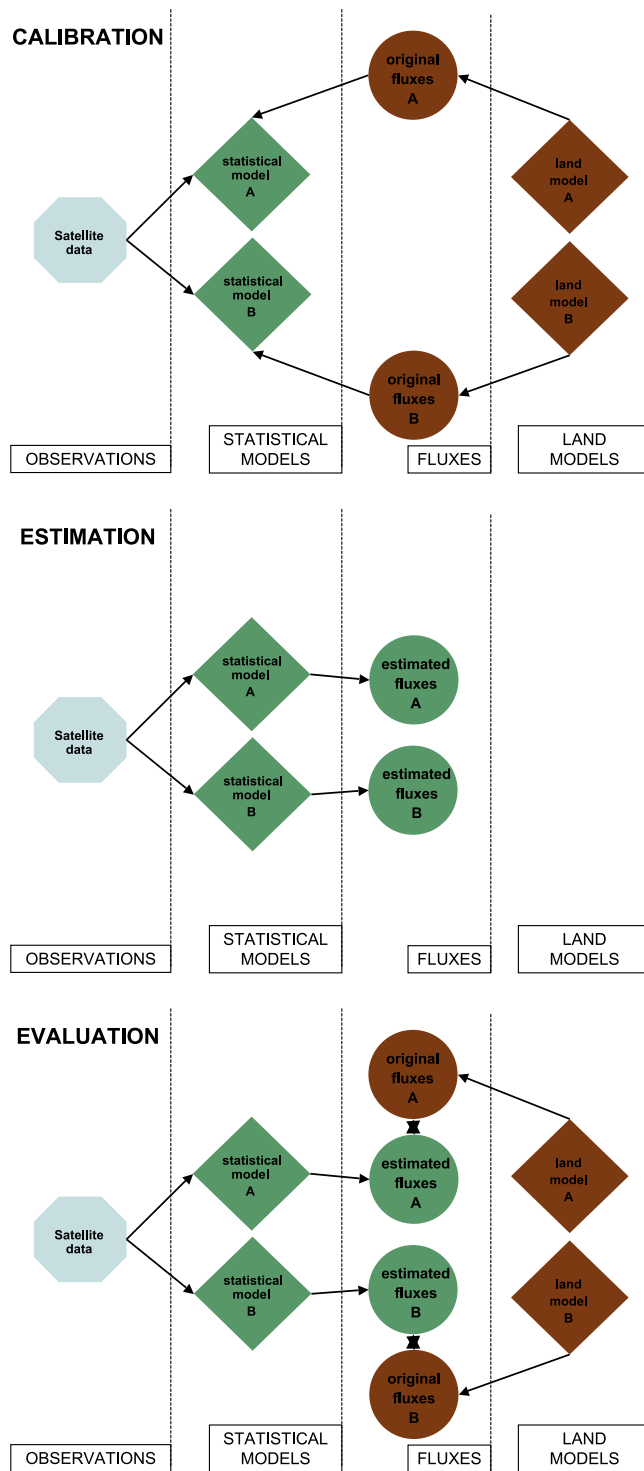


Figure 1. Different phases of the proposed methodology. In a first phase (calibration), a statistical model for each considered land model is calibrated with the satellite data and original land surface heat fluxes. In a second phase (estimation), the statistical models produce the estimated fluxes from the satellite data. In a third phase (evaluation), the original fluxes produced by the land models and the estimated fluxes produced by the statistical models are compared.

3.1. Global Land Surface Heat Fluxes

3.1.1. GSWP-2 Multimodel Analysis

[13] The GSWP is an international modeling research activity with the main goal of producing global data sets of soil moisture, other state variables, and related hydrological quantities using state-of-the-art LSMs [Dirmeyer *et al.*, 1999]. In the second phase of the project (GSWP-2) [Dirmeyer *et al.*, 2006], 15 LSMs driven in offline mode using global meteorological forcing inputs produced daily land fluxes and related surface variables for 10 years (1986–1995) at a resolution of $1^\circ \times 1^\circ$. The forcing, vegetation, and soil cover were primarily extracted from the ISLSCP Initiative 2 [Hall *et al.*, 2006], though elaborate work was undertaken to hybridize the reanalysis data with observational data in order to remove systematic errors [Zhao and Dirmeyer, 2003].

[14] In the study by Guo and Dirmeyer [2006], the GSWP-2 multimodel analysis resulting from a simple average across the individual models gave the best overall results when evaluating the modeled soil moisture outputs. This model ensemble is described as an analog to the atmospheric reanalysis, and judged as the best approach to combine the models, compared with more sophisticated combinations, in the absence of calibration data [Dirmeyer *et al.*, 2006]. In the present study, the link between satellite observations and fluxes will be mainly studied with the multimodel analysis, although individual runs from the participating models ISBA [Noilhan and Mahfouf, 1996] and ORCHIDEE [Krinner *et al.*, 2005] will also be considered for specific tests. The baseline integration run “B0” was first selected, as this is the run where most of the models took part.

3.1.2. NCEP/NCAR Reanalysis

[15] The NCEP/NCAR reanalysis (referred from now on as NCEP) is a retroactive record of more than 50 years of global atmospheric analyses produced by a frozen global data assimilation system [Kalnay *et al.*, 1996]. The land surface package of the NCEP reanalysis originated from the combination of the evaporation approach of Mahrt and Ek [1984], the multilayer soil model of Mahrt and Pan [1984], and the canopy model of Pan and Mahrt [1987]. A description of the model previous to its integration into the NCEP operational model can be found in the study by Chen *et al.* [1996]. The users of the NCEP reanalysis are warned that variables such as heat fluxes, humidity, or surface temperature should be interpreted with caution, as there are no assimilated observations to directly affect these variables. Evaluation of the NCEP heat fluxes at a regional scale can be found, for instance, in a comparison of the daily surface fluxes over grassland and boreal forests [Betts *et al.*, 1998], or in a comparison of the monthly mean fluxes with observations over the Southern Great Plains regions [Berbery *et al.*, 1999].

3.2. In Situ Land Surface Heat Fluxes

3.2.1. Marconi Data Set

[16] The FLUXNET Marconi Conference Gap-Filled Flux and Meteorology Data set was compiled for the FLUXNET 2000 Synthesis Workshop held in California in June 2000 [Falge *et al.*, 2005]. A total of 97 site-years of data were gathered, mainly between 1996 and 1998, including half-hour eddy covariance fluxes and meteorology

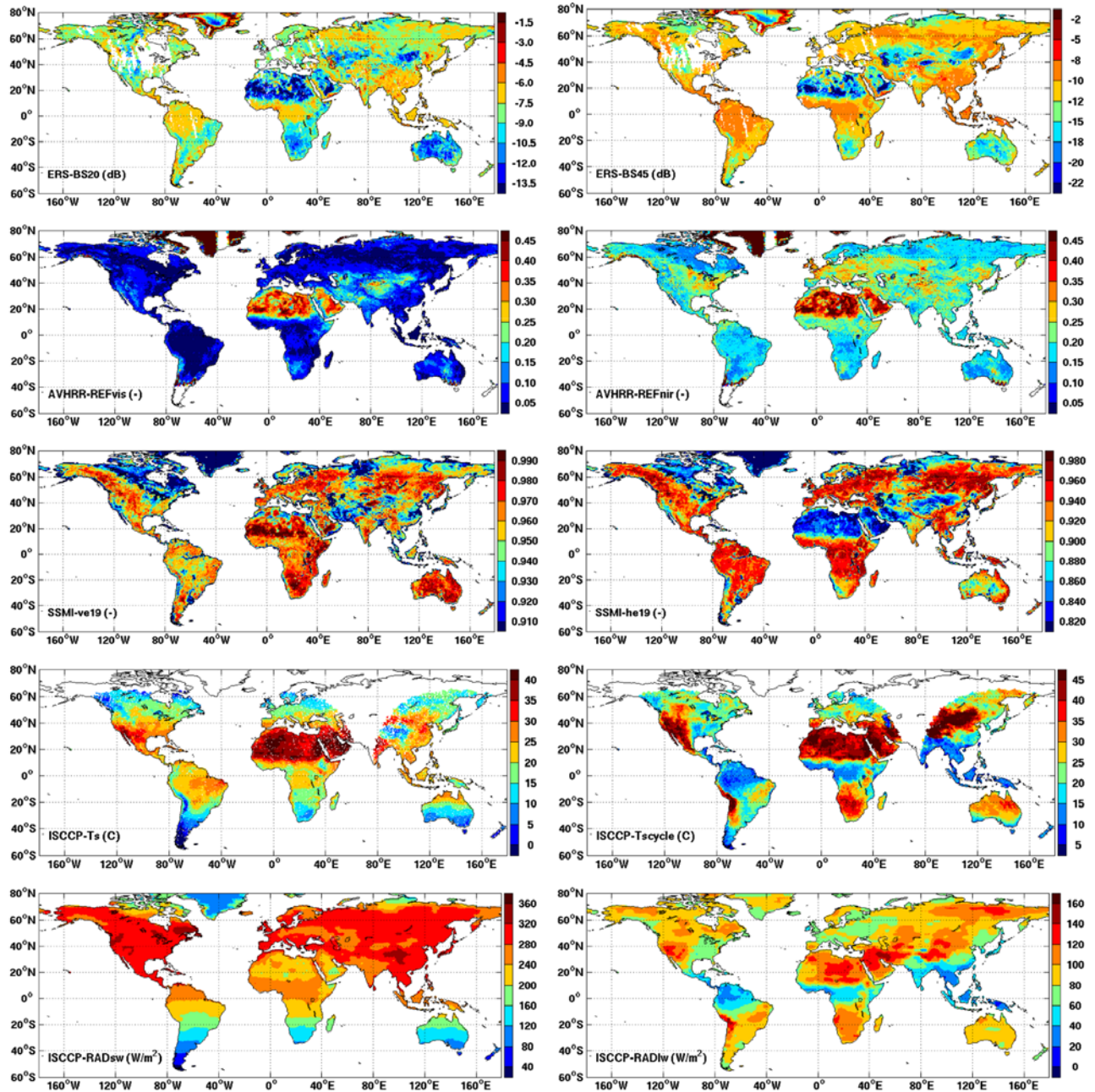


Figure 2. Examples of satellite data monthly means for June 1993: the ERS backscattering at 20° (ERS-BS20) and 45° (ERS-BS45), the AVHRR visible (AVHRR-REFvis) and infrared (AVHRR-REFnir) reflectances, the SSM/I emissivities from the vertically (SSMI-ve19) and horizontally (SSMI-he19) polarized 19 GHz channels, and the ISCCP skin temperature (ISCCP-Ts), its diurnal cycle (ISCCP-Tcycle), and the clear-sky net short-wave (ISCCP-RADsw) and long-wave (ISCCP-RADlw) radiation.

measurements and the gap-filled half-hour corresponding estimates and aggregations to longer time periods. Information about the product compilation and gap-filling techniques can be found at ftp://daac.ornl.gov/data/fluxnet/gap_filled_marconi/comp/Marconi_gapziips_website.pdf. The aggregated monthly means are used for the study.

3.2.2. AmeriFlux Data Set

[17] The AmeriFlux network is one of the regional networks integrated into the FLUXNET project. It was established in 1996 to understand the role of terrestrial systems in the global carbon cycle [Law *et al.*, 2002, AmeriFlux Strategic Plan available from http://public.ornl.gov/ameriflux/about-strategic_plan.shtml]. Over 100 sites are present in the network. Continuous measurements of fluxes are made by using the eddy covariance method. A good description of the eddy covariance flux measurements and their associated uncertainties and corrections needed in the context of the AmeriFlux network can be found in the study by *Massman and Lee* [2002]. The AmeriFlux web site has a well-documented and easily accessible archive, with data covering mostly the period 2000–2006, and this presented an opportunity to compile a new data set from the data of the individual stations. For this study the quality checked and standardized L2 data were downloaded.

3.3. Satellite Data

3.3.1. Visible and Near-IR: AVHRR Reflectances

[18] The AVHRR instruments on board the NOAA meteorological polar orbiters provide daily observations of the Earth with a resolution as high as 1 km. The first channel is in the visible, where chlorophyll causes absorption of incoming radiation, while the second one is in the near infrared. The Normalized Difference Vegetation Index (NDVI), based on the visible and near-infrared radiances, is extensively used for vegetation studies [e.g., *Moulin et al.*, 1997; *DeFries et al.*, 1999]. It is also integrated into some land surface heat flux estimation approaches to help characterize the relationship between fluxes and vegetation [e.g., *Carlson et al.*, 1995; *Nishida et al.*, 2003]. The product is described in detail in the study by *Gutman* [1999]. For this study the 10-day composite AVHRR products generated under the joint NASA and NOAA Earth Observing System Pathfinder Project [*James and Kalluri*, 1994], with a resolution of 8 km, were used. In this study, the visible and near-infrared radiances are used directly instead of the NDVI product, and the statistical method finds the best way of extracting the flux-related information from the radiances.

3.3.2. Thermal-IR: ISCCP Surface Skin Temperature and Its Diurnal Cycle

[19] The land surface skin temperature is a key variable in the determination of the heat fluxes. The most extensive data set of surface skin temperature is produced at 3 hour intervals since 1983 over the globe, every 30 km, by ISCCP [*Rossow and Schiffer*, 1999]. It combines all the infrared measurements from polar and geostationary operational weather satellites. For this study the surface skin temperatures were extracted from the ISCCP-DX product. *Aires et al.* [2004] developed a method to reconstruct the diurnal cycle of surface skin temperature for each location over the globe, based on a statistical analysis of the 3-hourly skin temperatures for clear scenes. The reconstructed skin tem-

peratures are averaged to provide the monthly temperature and to derive the amplitude of the temperature diurnal cycle. The IR surface estimates are limited to clear sky, meaning that the monthly mean skin temperatures and amplitudes are clear-sky biased. Depending on the cloudiness of each location, this can have an impact when estimating the monthly mean fluxes from these satellite products, as the original LSM fluxes are estimated from LSMs forced under the naturally occurring clear and cloudy conditions.

3.3.3. Active Microwaves: ERS Scatterometer Backscattering

[20] The European Remote-sensing Satellite ERS-1 was launched in 1991 and remained operational until 2001 [*Francis et al.*, 1991]. Its suite of instruments included a vertically polarized radar operating at C-band (5.3 GHz). This scatterometer was originally designed to measure near-surface winds over oceans, with a nominal resolution of 50 km, but it has also proved useful for land surface characterization [e.g., *Frison and Mougín*, 1996; *Schmullius*, 1997; *Magagi and Kerr*, 1997; *Wagner et al.*, 1999]. The signal relates to surface characteristics by the dependence of the backscatter with the soil and vegetation moisture, the vegetation coverage and type, and the surface roughness. The interplay between soil and vegetation is complex, but the incident angle of the backscatter has been found to allow some separation of the different contributions [*Frison and Mougín*, 1996]. *Prigent et al.* [2001a] also studied the sensitivity of the backscattering coefficient to vegetation, and *Prigent et al.* [2005] and *Aires et al.* [2005] evaluated its potential to estimate soil moisture. For this study, the backscattering coefficients were processed following a method similar to that of *Frison and Mougín* [1996], keeping the values at 20° and 45°

3.3.4. Passive Microwaves: SSM/I Emissivities

[21] The SSM/I instruments on board the Defense Meteorological Satellite Program (DMSP) polar orbiters observe the Earth twice daily at 19.35, 22.24, 37.00, and 85.50 GHz with both vertical and horizontal polarizations, with the exception of 22 GHz which is vertically polarized only. The observing incidence angle is close to 53° and the fields-of-view decrease with frequency, from $43 \times 69 \text{ km}^2$ to $13 \times 15 \text{ km}^2$ [*Hollinger et al.*, 1987]. The land microwave emissivities are estimated from SSM/I observations by removing contributions from the atmosphere, clouds, rain, and the surface temperature using ancillary data from ISCCP and the NCEP reanalysis [*Prigent et al.*, 1997, 2006]. In contrast to the direct use of the microwave brightness temperatures for surface characterization, these calculated emissivities are related to the surface properties themselves without confusing signals from atmospheric contribution or surface temperature variations. Their potential for surface characterization has been discussed in the study by *Prigent et al.* [2001b, 2005].

3.3.5. Net Radiation: ISCCP Radiative Fluxes

[22] Radiative fluxes are linked to the heat fluxes through the surface energy balance. Global estimates of the radiative fluxes are derived either from atmospheric reanalysis or from satellite retrievals. For this study, the products described in the study by *Zhang et al.* [2004] are selected (ISCCP-FD). This data set is an elaborated product, derived from a collection of global properties of clouds, atmosphere, and surface, used into a radiative transfer model to calculate

Table 1. Correlation Coefficients and RMS Errors for a Nonlinear Estimation Between Individual Groups of Satellite-Derived Variables and Sensible and Latent Fluxes (GSWP Multimodel Analysis and NCEP Reanalysis)^a

Satellite Products	Correlation		RMSE	
	GSWP	NCEP	GSWP	NCEP
<i>Sensible Flux</i>				
Emissivity	0.44	0.61	27.1 (58.1)	34.9 (63.0)
Backscatter	0.32	0.52	28.6 (61.3)	37.5 (67.7)
Reflectance	0.42	0.59	27.4 (58.8)	35.4 (63.8)
Skin Temperature	0.64	0.63	23.0 (49.5)	34.1 (61.6)
Diurnal Cycle	0.59	0.71	24.4 (52.3)	30.8 (55.5)
Net Radiation	0.69	0.70	21.8 (46.8)	31.5 (56.9)
<i>Latent Flux</i>				
Emissivity	0.80	0.83	21.6 (46.2)	31.5 (56.9)
Backscatter	0.70	0.75	25.6 (55.0)	36.7 (66.2)
Reflectance	0.82	0.79	20.2 (43.4)	34.5 (62.4)
Skin temperature	0.48	0.48	31.5 (67.7)	49.3 (89.1)
Diurnal cycle	0.72	0.76	24.9 (53.4)	36.2 (65.3)
Net radiation	0.82	0.84	20.6 (44.3)	29.5 (53.4)

^aThe satellite-derived variables are SSM/I emissivity, ERS backscatter, AVHRR reflectance, ISCCP skin temperature, amplitude of its diurnal cycle, and net radiation. The RMS error is given in W/m^2 and as a percentage of the mean flux (in brackets).

the radiative fluxes. The global cloud and surface properties are extracted from ISCCP, and the NASA Goddard Institute for Space Studies (GISS) radiative transfer model is employed for the calculations. It provides short-wave and long-wave, upwelling and downwelling fluxes at 5 levels between the top of the atmosphere and the surface, at 3 hour time steps and 280 km intervals.

4. Information Content of the Satellite Observations

4.1. Analysis for Individual Satellite Observations

[23] The study starts by comparing the fluxes from the GSWP multimodel analysis and the NCEP reanalysis with the fluxes estimated by individual statistical models linking the satellite observations and the GSWP or NCEP fluxes. For instance, for the SSM/I emissivity data, the statistical model is built with a NN having as inputs the 7 channels at different frequencies; for the IR skin temperature, the NN has only one input with skin temperatures; and so on. The statistical models are calibrated with data from February, May, August, and November 1993, as explained in section 2, while the correlation and errors are derived from the remaining data in 1993. Very similar statistics are obtained for 1994 or 1995. Global mean correlations and estimation errors are given in Table 1.

[24] For both sensible and latent fluxes the correlations with the net radiation are one of the strongest. This reflects the close relationship between radiative and heat fluxes through the surface energy balance, but it can also be due to cross-correlations between the radiation product and the LSM forcings. As the ISCCP radiative fluxes are quite an elaborated product requiring large ancillary data sets, it is difficult to assess the independence of this radiative fluxes from the LSM forcings. The downwelling short and long-wave components of the net radiation product from Zhang *et al.* [2004] used here are different from the downwelling

radiative fluxes by Stackhouse *et al.* [2004] used for the GSWP forcings, though they are still different estimates of a similar product. The skin temperature and the amplitude of its diurnal cycle are also highly correlated with the sensible fluxes (compared to the other satellite products): this reflects the close relationship between the sensible fluxes and the radiative surface temperature, as discussed in section 1. For the latent fluxes the AVHRR reflectances are next, but followed closely by the SSM/I emissivities and the amplitude of the surface temperature diurnal cycle. This is also expected: the difference between atmospheric and surface moisture controls the latent fluxes and the AVHRR reflectances, the SSM/I emissivities and the amplitude of the diurnal cycle have shown good correlations with vegetation and the available surface moisture, as discussed in section 3.3. However, for the particular case of the reflectances and the GSWP fluxes, the correlations should be interpreted with caution as some of the forcings related to vegetation are derived from NDVI time series. Note that this is not the case for the NCEP reanalysis, and the correlation is also relatively high. In general, the correlations with the latent fluxes are higher than with the sensible fluxes. This could be an indication that the processes modulating the latent fluxes are better captured by the satellite data, but also an indication that the sensible fluxes cannot be reproduced by the LSMs as well as the latent fluxes.

4.2. Analysis for Combinations of Satellite Observations

[25] The statistical model is now calibrated with all the satellite observations as inputs. The global mean correlations and estimation errors are given in Table 2 (“All Groups”). As expected, the statistical model using all

Table 2. Correlation Coefficients and RMS Errors for a Nonlinear Estimation Between Different Combinations of Individual Groups of Satellite-Derived Variables and the Sensible and Latent Fluxes (GSWP Multimodel Analysis and NCEP Reanalysis)^a

Satellite Products	Correlation		RMSE	
	GSWP	NCEP	GSWP	NCEP
<i>Sensible Flux</i>				
All groups	0.83	0.84	16.7 (36.0)	23.5 (42.4)
No emissivity	0.78	0.80	18.7 (40.2)	26.0 (46.9)
No backscatter	0.79	0.81	18.5 (39.7)	25.8 (46.5)
No reflectance	0.78	0.80	18.7 (40.0)	26.0 (47.0)
No skin temperature	0.69	0.75	21.9 (47.0)	29.1 (52.5)
No diurnal cycle	0.73	0.78	20.5 (44.0)	27.2 (49.2)
No net radiation	0.79	0.81	18.4 (39.6)	25.5 (46.1)
No rad no reflex	0.78	0.80	18.4 (39.3)	26.2 (47.2)
<i>Latent Flux</i>				
All groups	0.92	0.92	14.2 (30.5)	22.0 (39.7)
No emissivity	0.88	0.87	17.0 (36.6)	27.1 (48.9)
No backscatter	0.88	0.87	17.0 (36.3)	27.3 (49.2)
No reflectance	0.86	0.87	18.5 (39.7)	27.6 (49.9)
No skin temperature	0.87	0.87	17.9 (38.5)	27.5 (49.7)
No diurnal cycle	0.88	0.88	16.8 (36.2)	27.0 (48.7)
No net radiation	0.89	0.89	16.5 (35.4)	25.8 (46.7)
No rad no reflex	0.85	0.87	18.8 (40.4)	27.4 (49.5)

^a“All Groups” means with all the satellite variables listed in Table 1. “No variable *X*” means all variables but the variable *X*. The last case labeled as “No Rad No Reflex” corresponds to all variables but the net radiation and the reflectances (see the text for more details). The RMS error is given in W/m^2 and as a percentage of the mean flux (in brackets).

satellite products estimates the fluxes better than the statistical models using only one satellite product. The sensible flux relative errors are lowered approximately by 13% and 16% for the GSWP multimodel analysis and the NCEP reanalysis, respectively, and 15% and 12% for the latent fluxes. Then the individual satellite products are removed one by one, to evaluate how the newly calibrated statistical model with all inputs but one performs with respect to the all-inputs statistical model. The global mean correlations and estimation errors are given in Table 2 in the rows named as “No X”, where X is the satellite product removed. Removing the skin temperature has the largest impact on the sensible fluxes. For the latent fluxes, the information given by the different products seems more redundant. In principle, different statistical models with all satellite inputs but one could be calibrated and used to estimate the fluxes for those situations where one of the satellite products is absent. The case where both radiation and reflectances are not used as inputs to the statistical model is also given, to show that the capacity of the statistical model to estimate the multimodel fluxes is not just a consequence of cross-correlations between the NDVI LSM forcings and the AVHRR inputs. Even without those two inputs, the correlations and estimation errors are close to the case where only radiation was not used as an input.

5. Evaluation of the Satellite-Driven Fluxes

[26] In this section the capacity of a statistical model to estimate the land surface heat fluxes is evaluated. The statistical model has as inputs the SSM/I emissivities, the ERS backscatter, the AVHRR reflectances, the IR skin temperatures, and the diurnal cycle of the skin temperatures. The outputs are the sensible fluxes and the latent fluxes, and for each LSM one independent NN statistical model is calibrated with the corresponding satellite data and fluxes as described in section 2. The net radiation is not used as an input. As discussed in section 4.1, it is more likely to be correlated with the LSM forcing and a more complex product. This decision could be revised in the future for a given LSM and radiation product. The AVHRR reflectances could also be correlated with the vegetation forcing in the GSWP exercise, as also explained in section 4.1. Some of the analyses for the GSWP LSMs were rerun with and without the reflectances, and very similar statistics were obtained. In order to emphasize the synergy between the observations from the visible to the microwave, the AVHRR reflectances are kept as inputs to the statistical models.

5.1. Analyzing the Estimation Error

[27] The estimation error, the difference between the original LSM fluxes and the fluxes estimated by the statistical model, arises from different sources. Firstly, the link between the fluxes and the satellite observations can be established because some of the processes modulating the fluxes have a signature in the satellite measurements. However, a completely deterministic mapping between fluxes and satellite data cannot be expected as some of the processes affecting the fluxes are not captured by the satellite data. A second source of errors is related to the two data sets themselves: the fluxes produced by the LSMs will always be an approximation of the real fluxes, and the

satellite observations are also subject to errors, both instrumental errors and limitations or errors in the data processing. For instance, the skin temperature product is clear-sky biased. Even if there was a completely deterministic mapping between fluxes and satellite data and error-free flux observations and satellite data, a third source of error would come from the statistical model itself. The statistical model will always be an approximation of the processes to be modeled, even if it can be a very good one.

[28] The histograms of the fluxes estimated by the statistical model and the corresponding LSM fluxes are displayed in Figure 3. Starting with the sensible fluxes, the histograms show that the NCEP fluxes are different from the GSWP fluxes. The distributions from the estimated fluxes follow the shape of the original fluxes, though a narrowing of the distributions is visible. Extreme values are not well represented in the training data set (see the shapes of the LSM histograms), and as a consequence it is more difficult for the statistical model to reproduce those cases. Techniques exist where the original distribution is equalized in order to have all regions equally represented. In this case the calibration for the rare events is better, but at the expense of a poorer calibration for the more frequent events. Another possibility is to calibrate different statistical models for different regimes, as long as they can be recognized. This could be based on a geographical classification. These techniques could be considered for further developments.

[29] For the latent fluxes, the NCEP histogram looks also different from the GSWP histograms. The histograms show the same tendency to reduce the extreme values, but now only for the very large values or the very few negative values. Low positive values are now well represented in the data sets, and the errors for this part of the flux range do not increase (compared with the intermediate fluxes) as much as for the sensible fluxes.

5.2. Comparing Geographical and Temporal Patterns

[30] An example of the original and estimated monthly mean fluxes for the GSWP models, and the NCEP reanalysis is given in Figures 4 and 5 for August 1995. The data gaps in Figures 4 and 5 correspond to regions where some satellite inputs are not available. This happens essentially in central Asia, a region that was not covered by geostationary satellite at that time, and as a consequence, the diurnal cycle of the skin temperatures has not been calculated. The gaps could be filled by training the statistical model without this variable.

[31] Large efforts from the modeling community has led to comprehensive parameterization of the different processes and today the land surface heat fluxes derived from the models are the only realistic estimates at the global scale. Nevertheless, large differences can still be observed, in magnitude and geographical patterns, when comparing the original fluxes (left columns in Figures 4 and 5) even when they are equally forced LSMs (the multimodel, ISBA, and ORCHIDEE). For instance, significant differences between the ISBA and ORCHIDEE fluxes and their partitioning can be observed in the tropics. In general, there is a better agreement among the different LSMs themselves for the latent fluxes than for the sensible fluxes. The corresponding estimated fluxes by the statistical models are displayed in the right columns in Figures 4 and 5. The maps show that

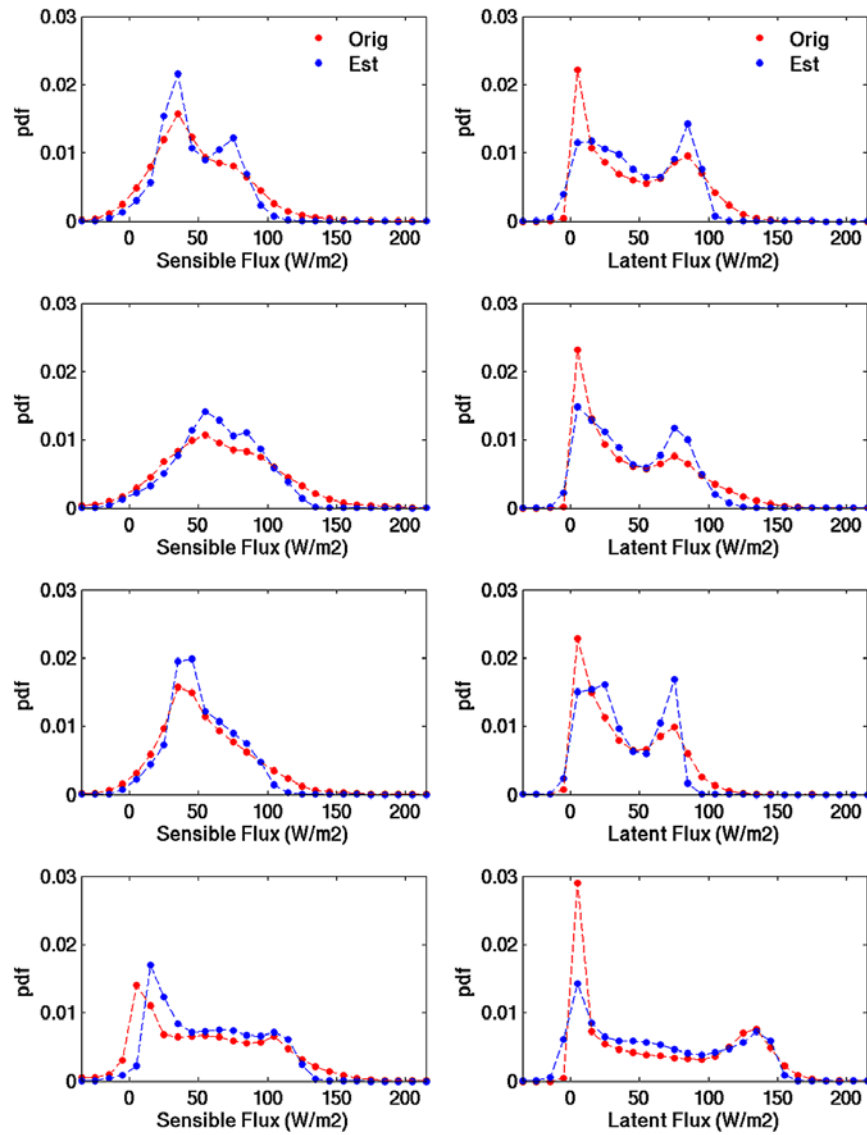


Figure 3. Histograms for the 1993–1994–1995 original (Orig) and estimated (Est) fluxes. The histograms of original (red) and estimated (blue) fluxes are plotted normalized to unity area. (left) Sensible fluxes. (right) Latent fluxes. (top to bottom) Fluxes for the multimodel analysis, ISBA, ORCHIDEE, and the NCEP reanalysis.

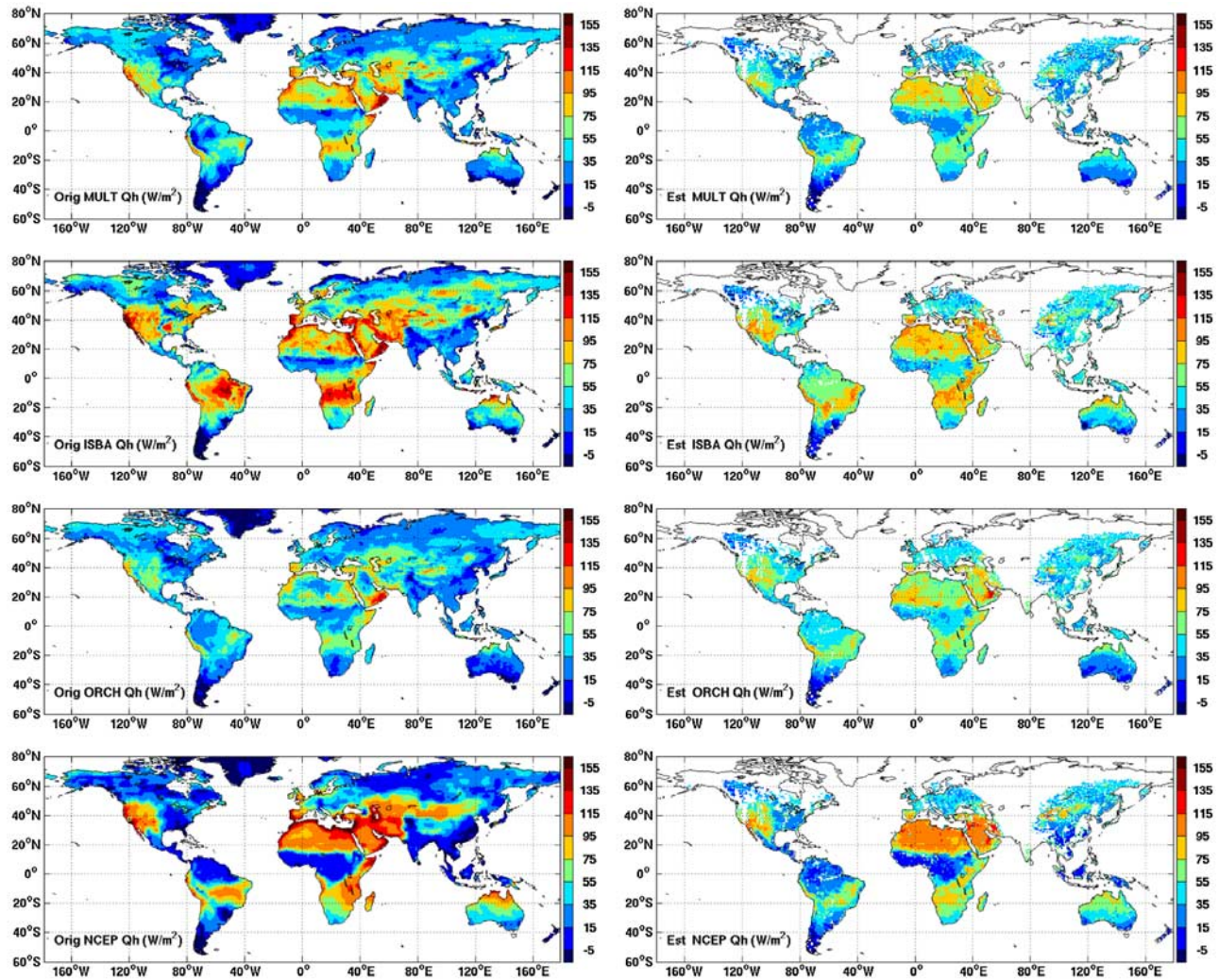


Figure 4. Example of estimated monthly mean sensible fluxes for August 1995. (Left) Original fluxes. (Right) Estimated fluxes. (Top to bottom) Fluxes for the multimodel analysis, ISBA, ORCHIDEE, and the NCEP reanalysis.

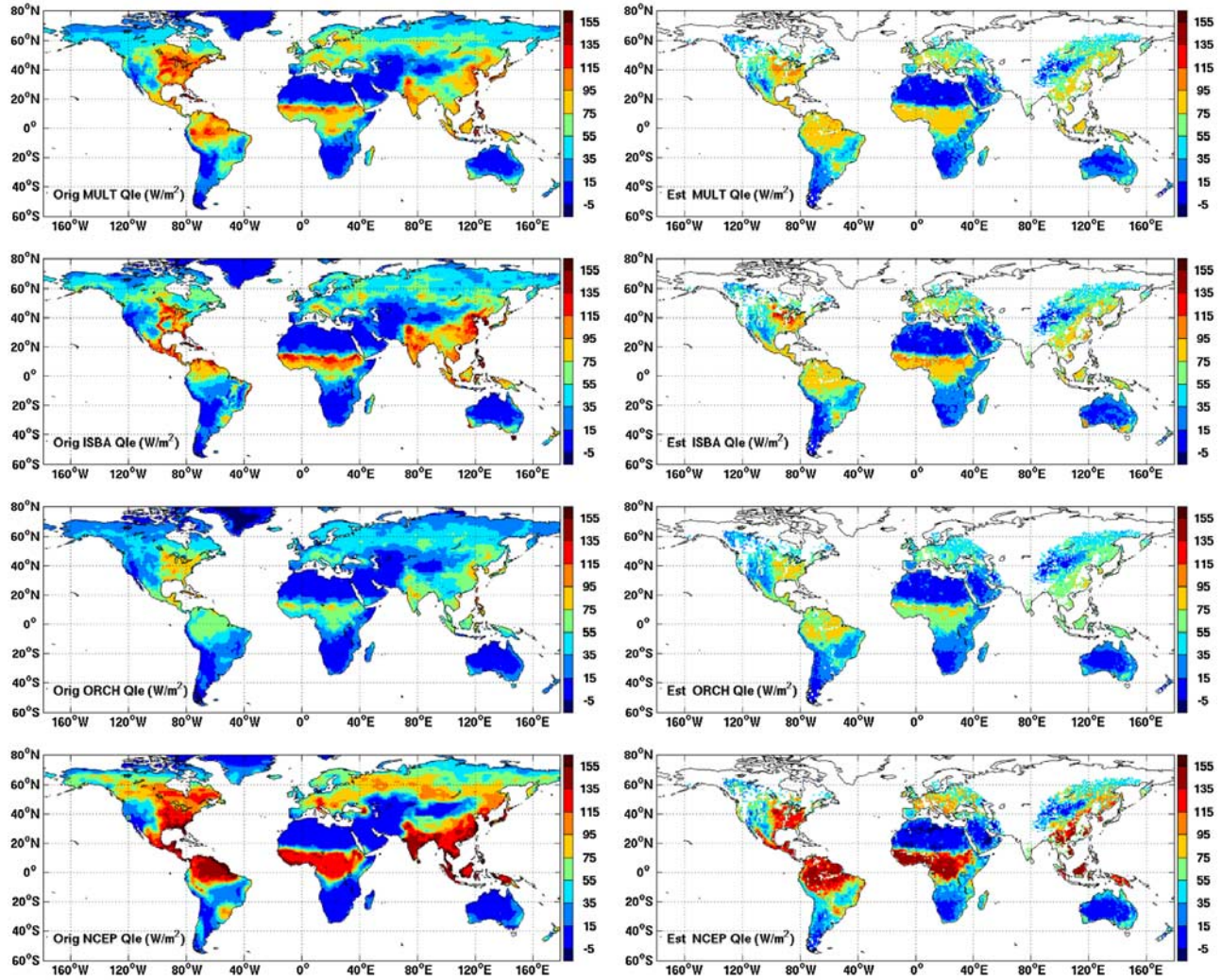


Figure 5. As in Figure 4 but for the latent fluxes.

Table 3. Comparison of the Multimodel Original and Satellite-Derived Sensible and Latent Fluxes (W/m^2) for Six Latitude Bands and 6 Months in 1994^a

	February	April	June	August	October	December	All Months
<i>Sensible Flux</i>							
40°N60°N	0.4 (5.1)	35.9 (37.0)	52.9 (39.1)	45.8 (42.3)	0.6 (4.8)	-11.8 (-6.5)	28.5 (27.3)
20°N40°N	26.2 (33.5)	65.5 (64.4)	74.7 (67.9)	70.2 (67.2)	32.8 (38.6)	7.7 (11.6)	44.4 (45.4)
0°20°N	65.7 (62.3)	66.3 (61.9)	58.4 (51.3)	47.9 (45.5)	40.7 (46.9)	44.3 (43.2)	54.5 (52.4)
20°S0°	39.5 (39.9)	33.4 (36.1)	30.6 (37.4)	52.5 (55.6)	59.4 (57.2)	45.4 (44.1)	44.2 (44.6)
20°S40°S	58.2 (64.0)	35.2 (43.5)	19.5 (35.3)	38.9 (53.0)	70.4 (66.3)	85.8 (69.9)	58.9 (58.4)
40°S60°S	69.1 (52.3)	-0.3 (15.0)			29.0 (36.3)	73.6 (57.4)	44.5 (38.8)
Global	45.8 (48.2)	49.1 (50.1)	50.3 (48.4)	54.5 (54.8)	44.6 (47.2)	42.6 (40.4)	48.1 (47.7)
<i>Latent Flux</i>							
40°N60°N	11.4 (17.4)	36.0 (27.2)	75.5 (67.5)	54.6 (63.9)	26.8 (32.1)	12.0 (21.0)	44.6 (46.4)
20°N40°N	16.3 (20.8)	26.2 (27.8)	31.4 (32.3)	30.0 (32.6)	23.8 (25.2)	11.4 (19.3)	22.1 (25.4)
0°20°N	33.4 (27.9)	47.9 (46.3)	54.0 (52.6)	66.5 (58.6)	63.0 (54.3)	46.5 (43.4)	51.3 (48.6)
20°S0°	85.4 (76.4)	78.3 (77.8)	54.9 (63.8)	47.4 (51.6)	59.9 (60.0)	79.7 (72.8)	67.8 (67.8)
20°S40°S	68.9 (54.5)	32.2 (45.1)	18.4 (31.0)	18.2 (21.0)	33.5 (36.9)	54.2 (47.3)	42.0 (43.0)
40°S60°S	37.3 (28.3)	36.6 (25.0)			39.4 (22.1)	53.4 (34.8)	41.0 (26.3)
Global	47.9 (45.6)	48.1 (49.6)	49.4 (52.0)	44.4 (46.5)	44.3 (43.5)	48.1 (46.0)	46.7 (47.0)

^aIn each cell, the first number gives the zonal value for the original fluxes, the number in brackets corresponds to the estimated fluxes. The last column gives the averaged fluxes over the 6 months for a given latitude band. The last row gives the globally averaged fluxes for a given month. The values at the right-bottom corner give the global mean fluxes for the 6 months considered.

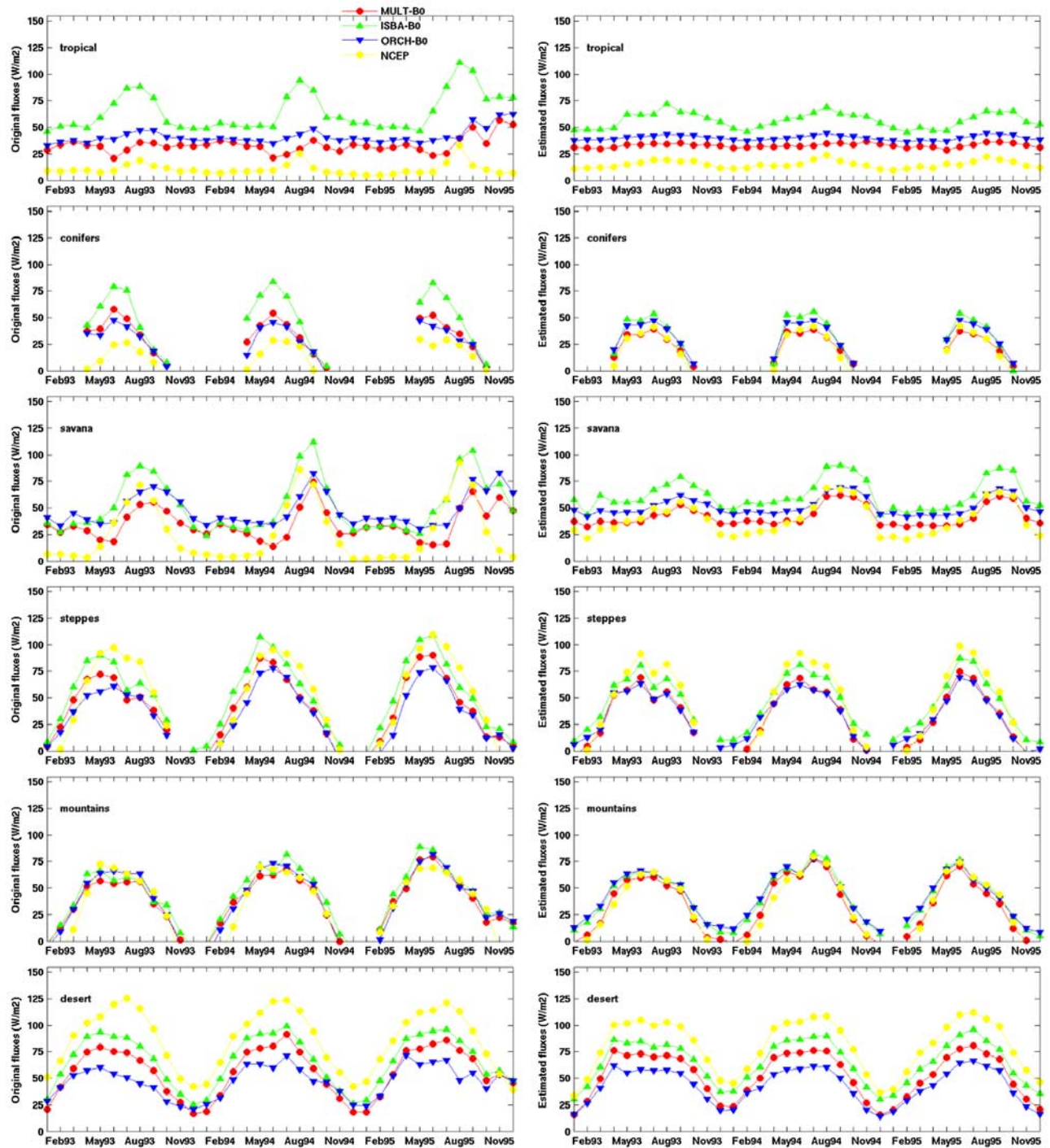


Figure 6. Examples of area averaged sensible fluxes for different regions. (Left) Averages for the original fluxes. (Right) Estimated fluxes. (Top to bottom) Fluxes corresponding to a tropical (10°S0°, 70W50°W) and savana (20°S10°S, 65°W40°W) regions in South America, coniferous forest (50°N60°N, 100°E40°E), steppes (40°N50°N, 90°E110°E) and mountain (30°N40°N, 80°E100°E) regions in Asia, and a desert region (20°N30°N, 10°E30°E) in North Africa. Shown fluxes from the multimodel analysis (red), ISBA (green), ORCHIDEE (blue), and the NCEP reanalysis (yellow).

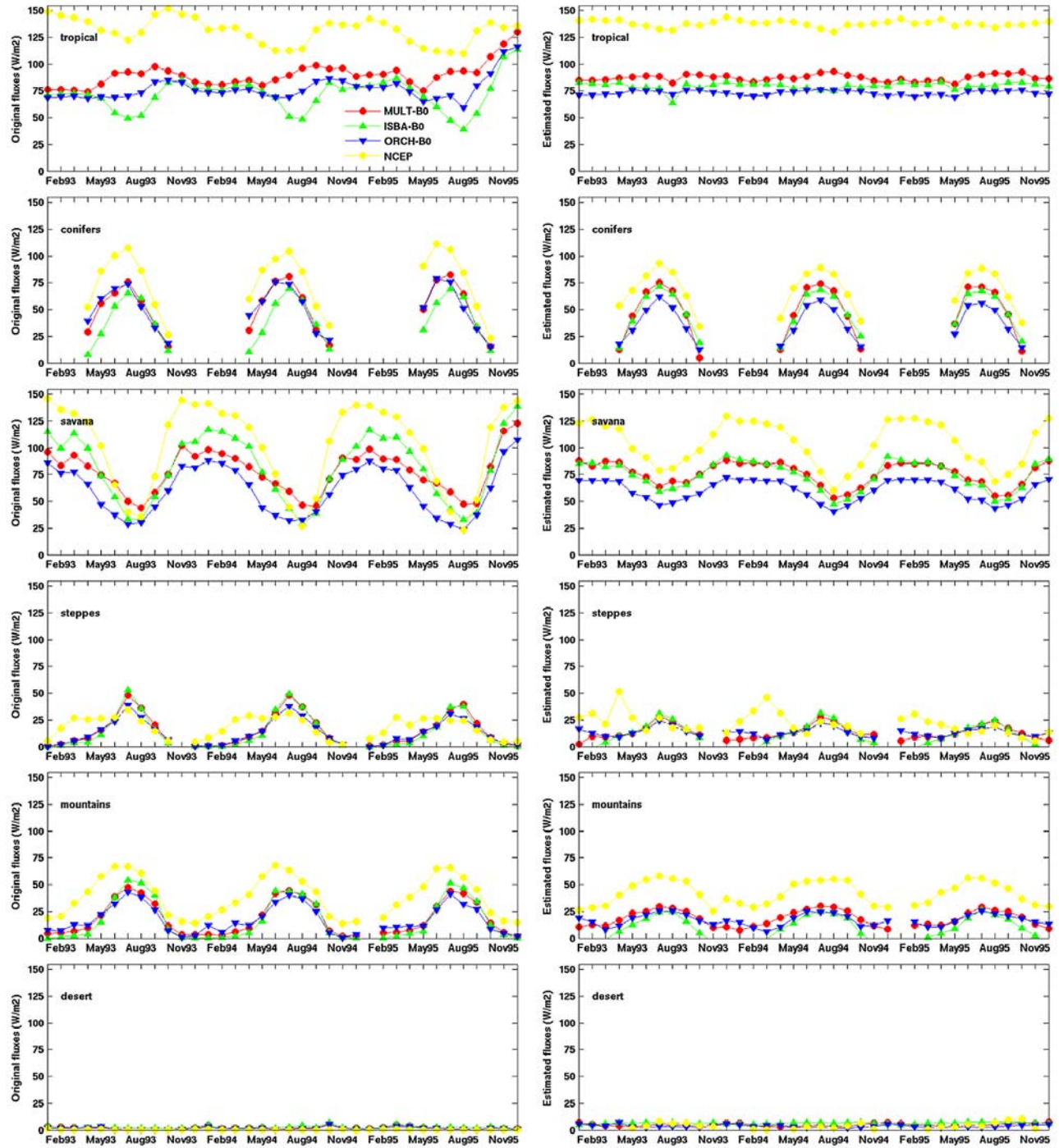


Figure 7. Same as in Figure 6 for the latent fluxes.

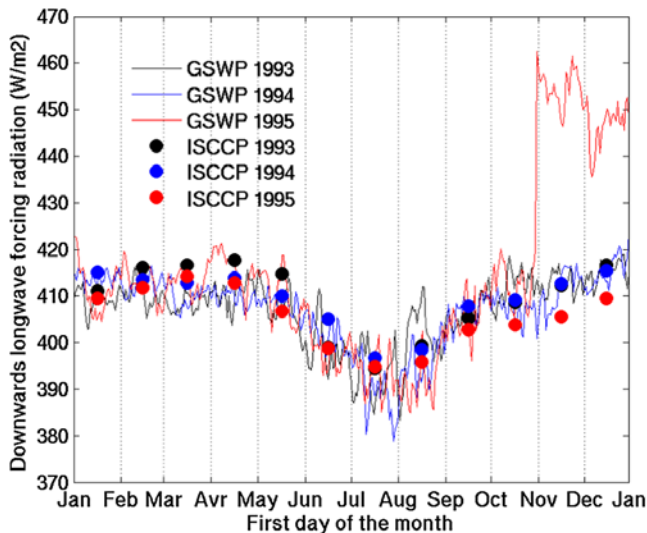


Figure 8. GSWP-2 downward long-wave radiative forcing. The daily mean values averaged in a $10^{\circ}\text{S}0^{\circ}$ latitude band over South America for 1993 (black), 1994 (blue), and 1995 (red) are plotted. For comparison, the ISCCP monthly mean values are also plotted for the same years as closed circles.

the estimated fluxes capture relatively well the regional variations associated to different climate and vegetation regimes, although some exceptions are visible. A more quantitative analysis is summarized in Table 3, where the multimodel original and estimated zonal mean fluxes for six different latitude bands and 6 months in 1994 are given. There are some dispersion between the original and estimated fluxes, but in general the zonal and monthly gradients are well reproduced by the statistical model. The largest differences are found for the $60^{\circ}\text{S}40^{\circ}\text{S}$ latitude band, which only includes a relatively small number of land pixels. Table 3 also gives the yearly averaged fluxes for a given latitude band, and the monthly averaged fluxes for the whole globe. Both yearly and monthly original and estimated averaged fluxes agree relatively well. The statistical model is calibrated to represent the global relationship between satellite data and fluxes, and will reproduce the original LSM global means.

[32] In order to analyze their time evolution, the fluxes from the multimodel analysis, the ISBA and ORCHIDEE models, and the NCEP reanalysis were averaged for a set of six regions with different vegetation covers over the 1993–1995 period. A comparison of the original LSM fluxes and the estimated fluxes by the statistical model is presented in Figures 6 and 7 for these regions. In general, the estimated fluxes capture the seasonal variations in all the regions, although in some cases there are noticeable differences between the original and estimated fluxes. The estimated fluxes agree better with each other than the original LSM fluxes themselves. This is clear particularly for the coniferous region. It could be argued that the statistical model tends to reduce the extreme values for a given model and ‘smooth’ the fluxes: consequently the estimations for the different models would tend to agree better. However, this can also be the consequence of the statistical model forcing the consistency between satellite data and the different LSM

estimates. If the estimated fluxes are a better estimate of the real fluxes, they are expected to be closer than the original LSM fluxes themselves.

[33] As said before, the statistical model cannot remove global biases. However, if there are specific regions with anomalous fluxes in disagreement with the global relationship, the statistical model can potentially identify these cases. For instance, the original ISBA fluxes in the Amazon region behave differently during summer, whereas the statistically reproduced ISBA fluxes are in better agreement with the fluxes from the other LSMs. A comparison with tower fluxes from a station in this region (see following section 5.3) seems to indicate anomalous ISBA fluxes for this part of the year. Another example is the large fluxes produced by the multimodel, ISBA, and ORCHIDEE in the last months of 1995 in the tropical and savana regions. The statistical models also modify those fluxes and estimate fluxes that agree better with the fluxes from the previous years. In this case, it was confirmed that the anomalous GSWP fluxes were the result of an anomaly in the radiative forcing of the models. Figure 8 plots the downward long-wave radiative forcing for the same latitude band in South America. The forcing anomaly was caused by a filling procedure that replaced the original radiative forcing that was missing for those months [Zhao and Dirmeyer, 2003]. In both examples the statistical model helps diagnose specific problems in the LSMs. However, a difference between original and estimated fluxes could also highlight a potential problem with the satellite data, or with the capacity of the statistical model to reproduce the fluxes in that region, so any differences between original and estimated fluxes have to be carefully interpreted.

5.3. Comparison With Tower Fluxes

[34] A validation of the original LSM fluxes and the fluxes estimated by the statistical model would be of great interest in order to see whether the statistical models driven by the satellite observations can reproduce more realistic fluxes than the original LSMs. However, this task is very challenging, especially at the global scale and for the period selected here. Spatially, comparison of point measurements from a flux tower with flux estimates averaged over a large area is a problem. Geographically, stations are concentrated in midlatitude regions, and as a consequence, do not represent global conditions. The largest differences between the model fluxes are precisely outside these relatively well characterized regions, such as the African deserts or the Amazonian forest (see Figures 4 and 5). Temporally, for all stations but one there is no data available for 1993–1995.

[35] The only station with a relatively long record of flux measurements is the Harvard forest station (42.5°N , 72.2°W), located in an area of temperate deciduous forest. Figure 9 shows a comparison of its tower monthly fluxes with the original and estimated monthly fluxes averaged over a $2^{\circ} \times 2^{\circ}$ longitude-latitude box around the station (smaller boxes were also tested, but without changing the conclusions of the comparison). Absence of LSM fluxes corresponds to snow periods or/and missing satellite data. Some gaps in the tower fluxes are also noted. The tower sensible fluxes show a large inter-annual variability and differ significantly from the LSM fluxes. Note also the large dispersion between the LSM sensible fluxes, even among

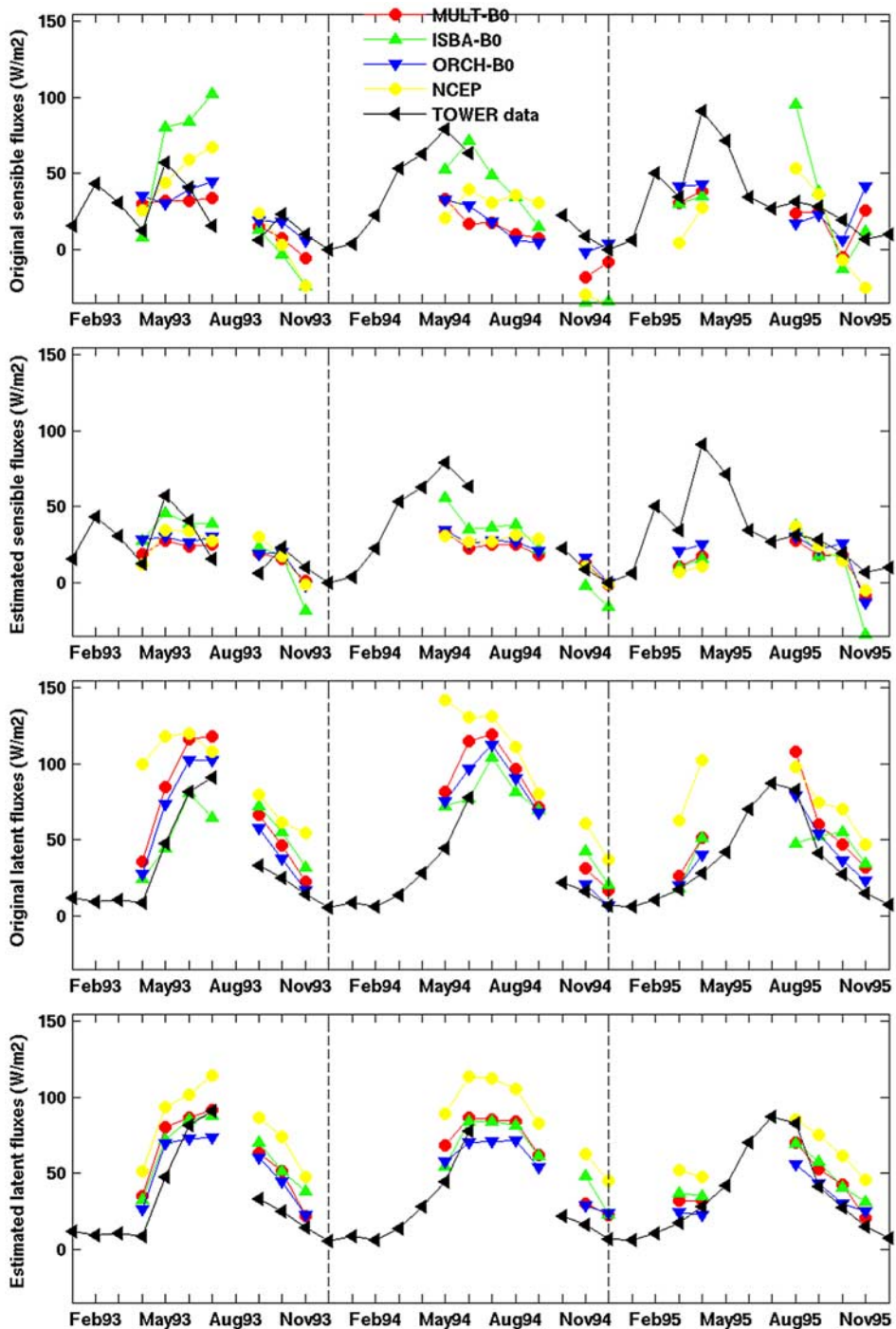


Figure 9. Averaged fluxes in a $2^\circ \times 2^\circ$ box around the Harvard Forest station. (Top to bottom) Original sensible fluxes, the estimated sensible fluxes, the original latent fluxes, and the estimated latent fluxes. Shown fluxes from the multimodel analysis (red), ISBA (green), ORCHIDEE (blue), the NCEP reanalysis (yellow), and the measurement tower (black).

Table 4. Correlation Coefficients and RMS Errors for the Comparison of the Multimodel, ISBA, ORCHIDEE, and NCEP Original and Satellite-Derived Estimated Fluxes With the Tower Fluxes From the Harvard Forest Station Plotted in Figure 9^a

	Correlation		RMSE (W/m ²)	
	LSM	SM	LSM	SM
	<i>Sensible Flux</i>			
MULT	0.57	0.57	25.2	26.2
ISBA	0.52	0.57	37.5	26.3
ORCH	0.47	0.56	23.8	24.5
NCEP	0.46	0.42	33.5	27.1
	<i>Latent Flux</i>			
MULT	0.97	0.91	25.5	17.6
ISBA	0.70	0.91	22.3	19.8
ORCH	0.95	0.87	15.6	15.3
NCEP	0.70	0.89	52.6	36.8

^aLSM refers to the original model fluxes; SM, to the fluxes estimated by each corresponding statistical model.

the original GSWP fluxes. The latent fluxes are in better agreement. The results are statistically summarized in Table 4. The worst agreement for the sensible fluxes is reflected in the lower correlations, compared with the latent fluxes. Even if the estimated sensible fluxes show less dispersion than the original fluxes, errors and correlations are not very different in general. For the latent fluxes, ISBA and NCEP fluxes are significantly less correlated than the fluxes from the multimodel and ORCHIDEE, and the satellite-derived fluxes for these models show better agreement with the tower fluxes. The correlations for the multimodel and ORCHIDEE were already over 0.9, and the statistical model seems to lower them slightly. However, this is just one example of an admittedly coarse comparison (specially in spatial terms) and no general conclusions can be derived.

[36] In order to extend the analysis further we also compared the surface fluxes with an annual climatology averaged over the existing years of tower data. This is again a coarse comparison, but for those locations where there is no large inter-annual variability it can nevertheless be illustrative. For example, for the measurements at the Tapajos national forest (2.9°S, 54.96°W) an annual climatology has been built by averaging the 2000–2006 fluxes, and these climatological fluxes are compared with the 1993–1995 LSM fluxes and the fluxes estimated by the statistical model over a 2° × 2° box around the station (Figure 10). An annual climatology is used, and as a consequence, each flux tower has an identical time series for each year. An idea of the inter-annual variability of the tower fluxes is given by plotting their monthly maximum and minimum for the years considered, showing that in this case the variability is relatively small compared with the mean climatological values. As observed with the Harvard forest fluxes, better agreement is found between the tower climatology and the LSM latent fluxes, compared with the LSM sensible fluxes. The NCEP sensible fluxes agree well with the climatology, but the latent fluxes are overestimated. The unusual behavior of the GSWP LSMs for the end of 1995 is not reproduced by the statistical models, as already discussed in section 5.2. Figure 11 presents the results at the Walnut Gulch Kendall grassland site (31.7°N, 109.9°W) in

Arizona. The seasonal amplitude of the original LSM sensible fluxes is larger than observed by the tower measurements, with also a significant inter-annual variability. The statistical models reproduce better the tower climatology and tend to yield fluxes with a reduced spread, compared to the large spread observed between the LSMs.

[37] In order to produce a more systematic comparison, the 1993–1995 fluxes and the 2000–2006 annual climatologies of 76 AmeriFlux stations and the 1996–1998 annual climatologies of 17 stations from the Marconi Conference data set have been compared. A box of 0.5° × 0.5° was used to match tower and modeled fluxes (the size of the box has been reduced, compared with the previous tests on individual stations, to allow a closer match between tower and model fluxes). This results in 798 matches for the AmeriFlux data set and 141 for the Marconi Conference data set. The Marconi Conference data set is processed with 4 different gap-filling techniques and the comparison is performed with the fluxes from the four techniques. For this particular comparison, slightly better agreement is found between the modeled fluxes and the climatological Marconi fluxes that use filling by mean daily courses (method MDC_orr). A summary of the comparison is given in Table 5 and Table 6 respectively for the AmeriFlux and Marconi (method MDC_orr) data sets. In general, the original LSM fluxes and the fluxes estimated by the statistical model compare similarly with the independent flux tower climatologies.

[38] The AmeriFlux data set results in a larger number of matches and is analyzed further. Histograms showing the distribution of the errors for the AmeriFlux comparison are plotted in Figure 12, and the mean and standard deviation of the differences are given in Table 7. The histograms for the differences between the AmeriFlux fluxes and the original and estimated fluxes are quite similar. No significant differences are found between the biases for the original and estimated fluxes. The global relationships should hold for these relatively well characterized midlatitude environments, and the statistical models cannot remove any biases if they exist, as discussed in section 5.2. Regarding the sign of the biases, all the models and the reanalysis sensible fluxes are negatively biased with respect to the AmeriFlux climatology, while for the latent fluxes all but ORCHIDEE are positively biased.

[39] As already said, this comparison is limited to the midlatitude regions, where most LSMs have been carefully studied, and no general conclusion can be drawn. The largest differences between the LSMs or between the original LSM fluxes and the fluxes estimated by the statistical models are not observed in these regions. For the transition regions where the LSMs may not capture correctly all the spatial and temporal variability, we would argue that the statistical models driven by the satellite data could be more efficient in terms of capturing this variability, but this cannot be demonstrated here with the analyzed flux tower data sets.

6. Conclusions

[40] The potential of a suite of satellite observations to estimate the latent and sensible heat fluxes over snow-free continents has been evaluated, using a methodology based

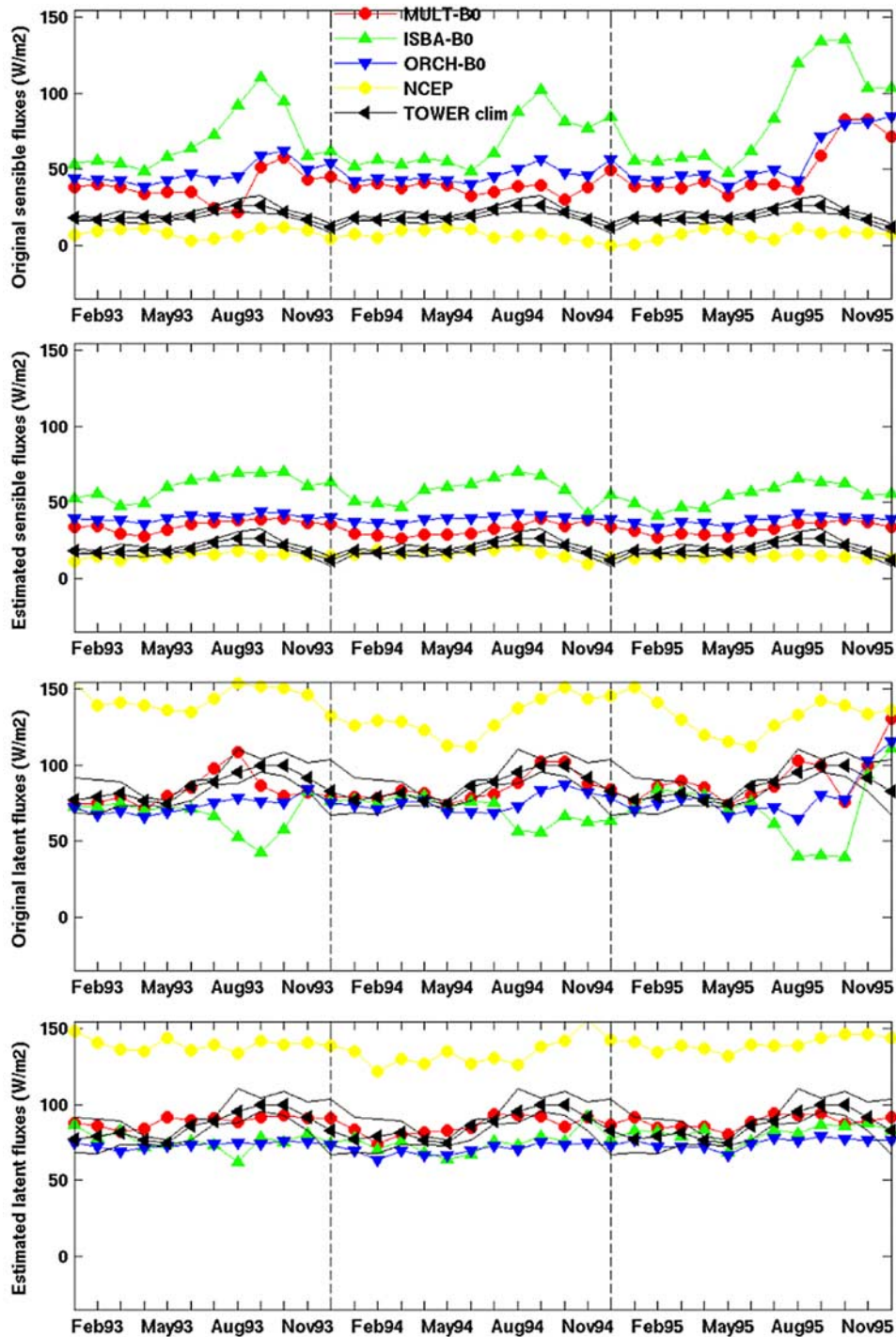


Figure 10. Same as in Figure 9 but around the Tapajos National Forest (primary forest station) and with the flux tower data corresponding to an annual climatology built by averaging the tower fluxes over the 2002–2006 period (see the text for more details). The black solid line represents the tower monthly maximum and minimum fluxes for that period.

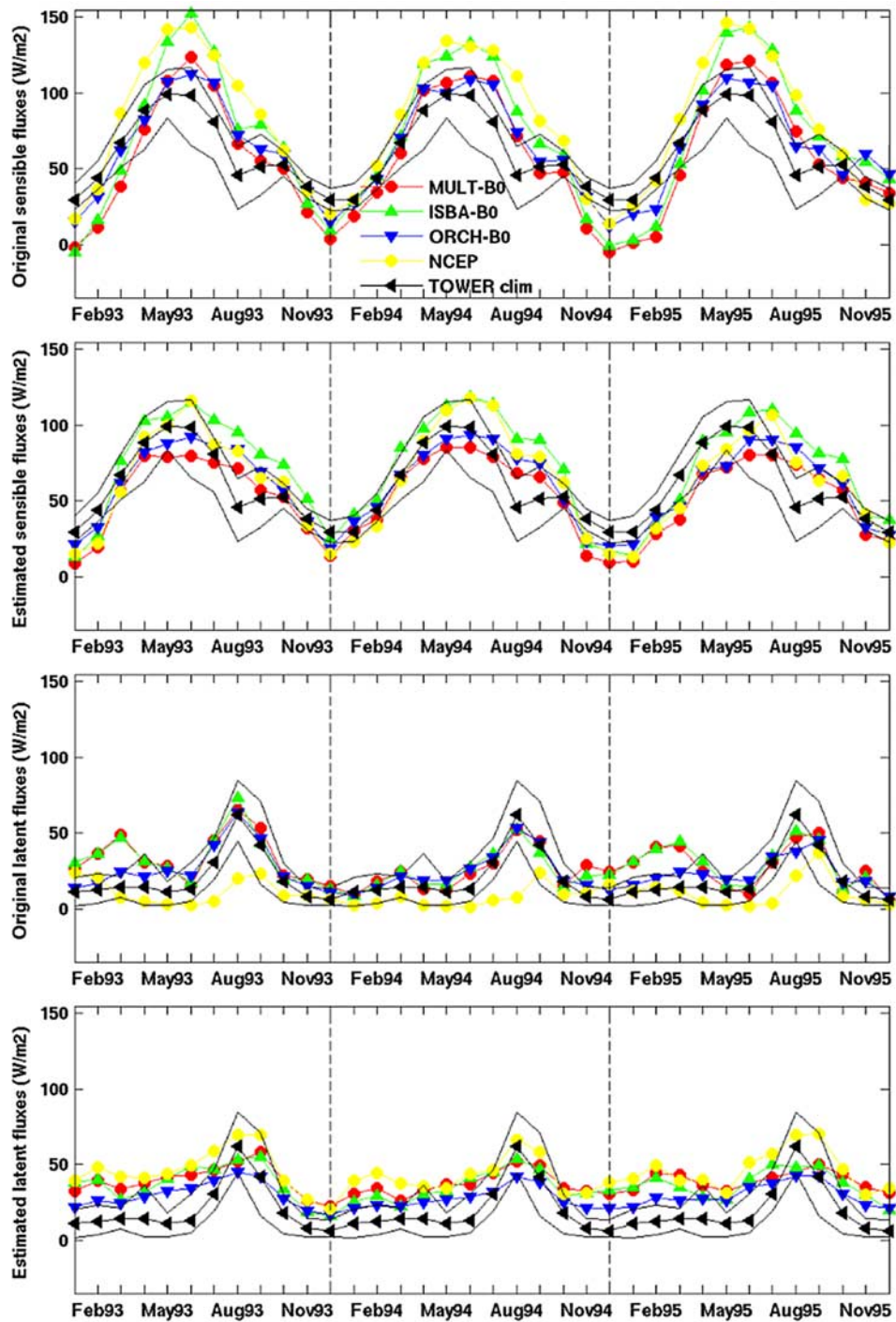


Figure 11. Same as in Figure 10 but for the Walnut Gulch Kendall station in Arizona and a 2005–2006 tower flux annual climatology.

Table 5. Comparison of the Fluxes From the Multimodel, ISBA, ORCHIDEE, and NCEP Models With Tower Fluxes^a

	Correlation		RMSE (%)	
	LSM	SM	LSM	SM
<i>Sensible Flux</i>				
MULT	0.66	0.68	66.3	59.1
ISBA	0.64	0.68	78.5	68.0
ORCH	0.70	0.67	51.8	52.8
NCEP	0.73	0.67	66.7	58.5
<i>Latent Flux</i>				
MULT	0.77	0.78	56.8	46.9
ISBA	0.70	0.71	58.0	55.0
ORCH	0.82	0.79	40.4	47.8
NCEP	0.76	0.75	72.0	64.4

^aThe table corresponds to a comparison with a 2000–2006 annual climatology from AmeriFlux data. LSM refers to the original model fluxes; SM, to the fluxes estimated by each corresponding statistical model. The correlation between model and tower fluxes is given, together with the RMS error of the differences between model and tower fluxes, expressed as percentage of the tower fluxes (see the text for more details).

on calibrating a statistical method linking a suite of satellite observations to the fluxes. The statistical model learns the global relationship between satellite data and fluxes, and can then be used to produce satellite-driven fluxes. The satellite data have been selected for their known sensitivity to the surface properties that affect the fluxes (soil moisture, surface temperature and its diurnal cycle, vegetation) as well as for their global coverage and their availability over many years. They cover a broad range of wavelengths from the visible to the microwaves. The in situ flux measurement being very scarce in space and time, the fluxes calculated from land surface models (LSMs) are adopted as the most reliable estimates of land surface heat fluxes at a global scale. GSWP outputs are selected, along with NCEP reanalysis. Three estimates from GSWP are studied: the multimodel, ISBA, and ORCHIDEE. The model and satellite data are gridded on a $0.25^\circ \times 0.25^\circ$ grid and averaged over a month, for the 1993–1995 period.

[41] The statistical links between the satellite data and the different LSM fluxes are analyzed using statistical models based on neural networks. The analyses are conducted separately for the four LSMs (three GSWP LSMs and the NCEP reanalysis), setting independent statistical models for each combination of satellite observations and LSM. The statistical models that use all the considered satellite observations as inputs can reproduce the modeled land fluxes on a global scale with theoretical RMS errors $<25 \text{ W/m}^2$, proving that the satellite data contain relevant information for flux estimation. The spatial and temporal patterns of the fluxes are well captured in general, although exceptions exist. Our analysis shows that individual satellite information cannot yield such results: the synergetic use of various wavelengths with complementary sensitivity improves the ability to reproduce the fluxes for all types of environments. The use of multiple satellite information also makes the scheme more robust to the lack of one specific observation, and the accuracy of the method with missing data has also been assessed.

[42] The LSM fluxes (original fluxes) and the satellite-derived estimates (estimated fluxes) have been qualitatively

evaluated. Comparisons of the original fluxes from the four land surface models (multimodel, ISBA, ORCHIDEE, and NCEP) revealed that in some regions the differences could be large, both in terms of magnitude and spatial structures. This is especially significant for the sensible fluxes, even when the models share the same forcing, as for the multimodel, ISBA, and ORCHIDEE. The statistical model cannot remove existing biases at the global scale, but for specific regions where there is a departure from the global relationship, the statistical model can potentially produce local fluxes that are more consistent with the learned global relationships. For instance, the comparison between original fluxes and estimated fluxes at the end of 1995 evidenced an anomaly in the GSWP radiation forcing fluxes. This scheme can thus help diagnose specific problems with the LSMs, though any discrepancies between original and estimated fluxes have to be also evaluated in the context of possible observation artifacts or errors introduced by the statistical model.

[43] It is very difficult to globally assess the accuracy of both original and estimated fluxes. A quantitative analysis has been attempted by comparing the original and estimated fluxes to independent available flux tower measurements. The comparison is of limited significance in the context of a global estimation of fluxes, as the geographical coverage of the tower data is almost limited to midlatitude environments. The largest differences between the LSM fluxes are observed outside these regions, where the LSMs have more difficulties to estimate the fluxes. Spatially, the comparison is rather coarse, as flux point measurements are compared with fluxes averaged over large areas. Temporally the comparison is rather limited, as only one station in a temperate deciduous forest was found to have data during 1993–1995. Comparison of the tower and LSM fluxes at this station showed that latent fluxes were more accurately modeled than the sensible fluxes, and no significant improvements were observed when comparing with the satellite-derived fluxes. In order to extend the comparison, a climatology of the tower flux measurements have been produced and compared with the flux estimates. Examples tend to show that adding the satellite information improved the modeled values when the differences between the LSM and tower fluxes are large, but a systematic comparison with all the available stations did not statistically prove it. As stated before, this exercise is essentially limited to midlat-

Table 6. As in Table 5 but for a Comparison With a 1996–1998 Annual Climatology From the Marconi Conference Data

	Correlation		RMSE (%)	
	LSM	SM	LSM	SM
<i>Sensible Flux</i>				
MULT	0.62	0.65	56.8	56.3
ISBA	0.65	0.61	97.5	86.8
ORCH	0.60	0.62	52.3	58.1
NCEP	0.54	0.60	84.7	65.7
<i>Latent Flux</i>				
MULT	0.73	0.75	55.5	42.2
ISBA	0.58	0.65	53.1	46.8
ORCH	0.74	0.69	40.3	37.5
NCEP	0.55	0.65	99.0	87.0

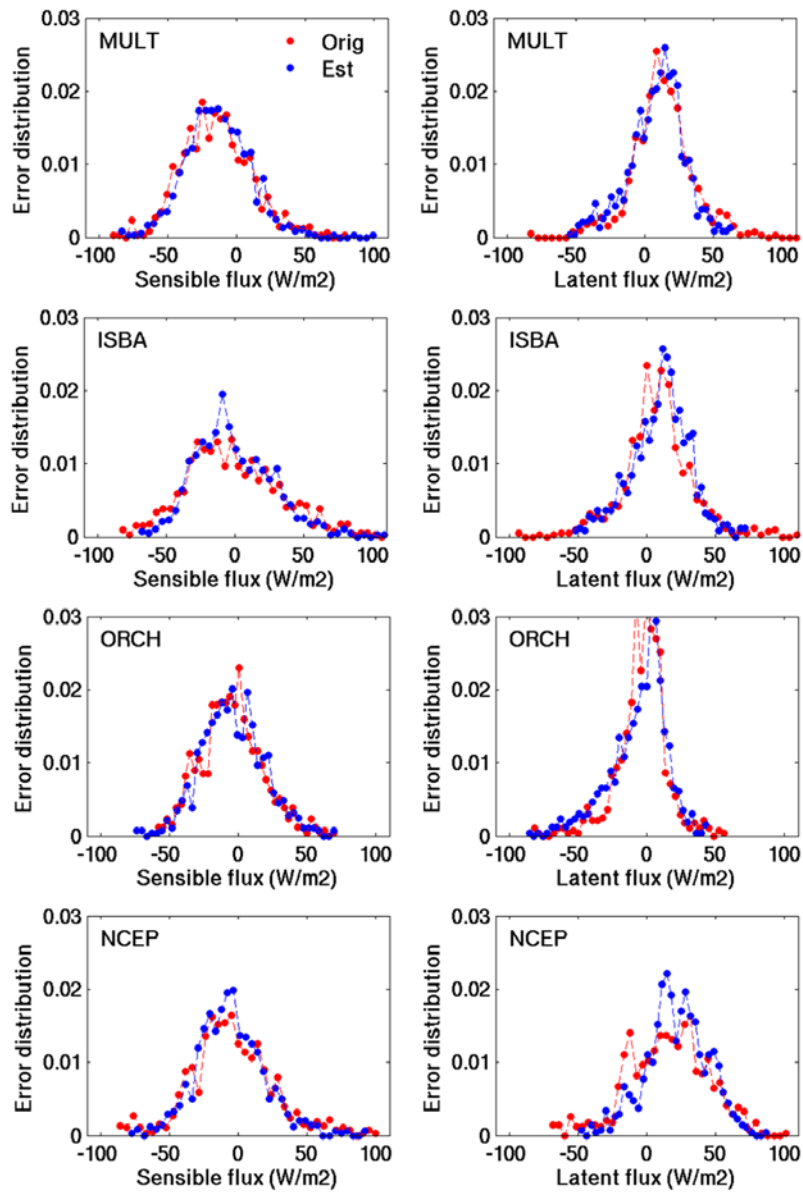


Figure 12. Histograms of the differences between the AmeriFlux climatologies and the modeled fluxes summarized in Table 7. The histograms of original (red) and estimated (blue) fluxes are plotted normalized to unity area. (Left) Sensible fluxes. (Right) Latent fluxes. (Top to bottom) Fluxes for the multimodel analysis, ISBA, ORCHIDEE, and the NCEP reanalysis.

Table 7. Absolute Means and Standard Deviations of the Error Distributions Plotted in Figure 12 for the Comparison Between Original and Estimated Fluxes With the 2000–2006 Annual Climatology From AmeriFlux Data^a

	Mean (W/m ²)		SD (W/m ²)	
	LSM	SM	LSM	SM
	<i>Sensible Flux</i>			
MULT	−14.6	−12.0	25.2	23.1
ISBA	−1.2	−1.6	34.5	29.9
ORCH	−5.0	−2.5	22.3	23.1
NCEP	−4.5	−4.8	30.3	25.3
	<i>Latent flux</i>			
MULT	12.6	7.7	22.4	19.8
ISBA	7.8	10.6	25.0	22.5
ORCH	−3.6	−6.7	17.9	20.6
NCEP	15.3	20.0	28.9	21.2

^aLSM refers to the original model fluxes; SM, to the fluxes estimated by each corresponding statistical model.

itude areas and cannot be conclusive in the context of a global comparison. The extension of the exercise to other regions remains very challenging in the absence of validation data, and the arguable superiority of the proposed methodology in those regions could not be demonstrated here.

[44] In a broad sense the proposed methodology can be considered similar in nature to an assimilation scheme [Aires *et al.*, 2005]: it combines satellite observations and model estimation to maximize consistency. Our methodology bypasses the actual estimation of the true land estate (e.g., soil moisture) and directly estimates heat fluxes without using a physical relationship, but a statistically derived relationship linking satellite observations and LSM outputs. As the methodology is tightly related to LSM outputs, it cannot be considered as a method to derive independent land surface heat fluxes from satellite observations. However, given the lack of any other reliable methodology at a global scale, it is a promising and pragmatic step forward, and a contribution toward the goal of deriving a global climatology of land surface fluxes, within the LANDFLUX initiative.

[45] **Acknowledgments.** We would like to thank Nicolas Enjalbert (Ecole Polytechnique) for participating in the early stages of this work, Bill Rossow (CREST, City College of New York) and Anton Beljaars (ECMWF) for general discussions about this work, and Katia Laval and Tristan d'Orgeval (Laboratoire de Météorologie Dynamique, Université de Paris), Hervé Douville and Bertrand Decharme (Météo-France), and Nicolas Viovy and Nathalie de Noblet (Laboratoire des Sciences du Climat et l'Environnement) for fruitful discussions concerning the land surface models. All data providers are acknowledged for making their data available. The ERS scatterometer data have been provided by IFREMER. The GSWP-2 data were downloaded from the GSWP Web site. The Marconi data set was obtained from the ORNL DAAC through the FLUXNET Web site, and the AmeriFlux data set was from the CDIAC ftp server through the AmeriFlux Web site. We would also like to thank five anonymous reviewers for their careful reading of the article and constructive suggestions.

References

Abramowitz, G. (2005), Towards a benchmark for land surface models, *Geophys. Res. Lett.*, **32**, L22702, doi:10.1029/2005GL024419.

Abramowitz, G., H. Gupta, A. Pitman, Y. Wang, R. Leuning, H. Cleugh, and K. Hsu (2006), Neural error regression diagnosis (NERD): A tool for model bias identification and prognostic data assimilation, *J. Hydrol.*, **7**, 160–177.

Abramowitz, G., A. Pitman, H. Gupta, E. Kowalczyk, and Y. Wang (2007), Systematic bias in land surface models, *J. Hydrol.*, **8**, 989–1001.

Aires, F., and C. Prigent (2006), Toward a new generation of satellite surface products?, *J. Geophys. Res.*, **111**, D22S10, doi:10.1029/2006JD007362.

Aires, F., C. Prigent, W. Rossow, and M. Rothstein (2001), A new neural network approach including first-guess for retrieval of atmospheric water vapor, cloud liquid water path, surface temperature and emissivities over land from satellite microwave observations, *J. Geophys. Res.*, **106**, 14,887–14,907.

Aires, F., C. Prigent, and W. Rossow (2004), Temporal interpolation of global surface skin temperature diurnal cycle over land under clear and cloudy conditions, *J. Geophys. Res.*, **109**, D04313, doi:10.1029/2003JD003527.

Aires, F., C. Prigent, and W. Rossow (2005), Sensitivity of satellite microwave and infrared observations to soil moisture at a global scale: 2. Global statistical relationships, *J. Geophys. Res.*, **110**, D11103, doi:10.1029/2004JD005094.

Anderson, M., J. Norman, J. Mecikalski, J. Otkin, and W. Kustas (2007), A climatological study of evapotranspiration and moisture stress across the continental United States based on thermal remote sensing. 1: Model formulation, *J. Geophys. Res.*, **112**, D10117, doi:10.1029/2006JD007506.

Baldocchi, D., et al. (2001), FLUXNET: A new tool to study the temporal and spatial variability of ecosystem-scale carbon dioxide, water vapor, and energy flux densities, *Bull. Am. Meteorol. Soc.*, **82**(11), 2415–2434.

Berbery, E. H., K. E. Mitchell, S. Benjamin, T. Smirnova, H. Ritchie, R. Hogue, and E. Radeva (1999), Assessment of land surface energy budgets from regional and global models, *J. Geophys. Res.*, **104**, 19,329–19,348.

Betts, A., J. Ball, A. Beljaars, M. Miller, and P. A. Viterbo (1996), The land surface-atmosphere interaction: A review based on observational and global modeling perspectives, *J. Geophys. Res.*, **101**(D3), 7209–7226.

Betts, A., P. Viterbo, A. Beljaars, H. Pan, S. Hong, M. Goulden, and S. Wofsy (1998), Evaluation of the land-surface interaction in the ECMWF and NCEP/NCAR reanalyses over grassland (FIFE) and boreal forest (BOREAS), *J. Geophys. Res.*, **103**, 23,079–23,085.

Bourras, D., L. Eymard, and W. T. Liu (2002), A neural network to estimate the latent heat flux over oceans from satellite observations, *Int. Remote Sens. J.*, **23**(12), 2405–2424.

Caparrini, F., F. Castelli, and D. Entekhabi (2004), Variational estimation of soil and vegetation turbulent transfer and heat flux parameters from sequences of multisensor imagery, *Water Resour. Res.*, **40**, W12515, doi:10.1029/2004WR003358.

Carlson, T. N., W. J. Capehary, and R. R. Gillies (1995), A new look at the simplified method for remote sensing of daily evapotranspiration, *Remote Sens. Environ.*, **54**, 161–167.

Cashion, J., V. Lakshmi, D. Bosch, and T. Jackson (2005), Microwave remote sensing of soil moisture: Evaluation of the TRMM microwave imager (TMI) satellite for the Little River Watershed Tifton, Georgia, *J. Hydrol.*, **307**(1–4), 242–253.

Chen, F., K. Mitchell, J. Schaake, Y. Xue, H. Pan, V. Koren, Q. Duan, Y. Ek, and M. Betts (1996), Modeling of land surface evaporation by four schemes and comparison with FIFE observations, *J. Geophys. Res.*, **101**, 7251–7268.

Coudert, B., C. Otté, B. Boudevillain, J. Demarty, and P. Guillevic (2006), Contribution of thermal infrared remote sensing data in multi-objective calibration of a dual source SVAT model, *J. Hydrometeorol.*, **7**, 404–420.

Crow, W. T., E. F. Wood, and M. Pan (2003), Multiobjective calibration of land surface model evapotranspiration predictions using streamflow observations and spaceborne surface radiometric temperature retrievals, *J. Geophys. Res.*, **108**(D23), 4725, doi:10.1029/2002JD003292.

DeFries, R. S., J. R. G. Townshend, and M. C. Hansen (1999), Continuous fields of vegetation characteristics at the global scale at 1-km resolution, *J. Geophys. Res.*, **104**, 16,911–16,923.

Dirmeyer, P. A. D., A. Dolman, and N. Sato (1999), The pilot phase of the Global Soil Wetness Project, *Bull. Am. Meteorol. Soc.*, **80**, 851–878.

Dirmeyer, P. A., X. Gao, M. Zhao, Z. Guo, T. Oki, and N. Hanasaki (2006), GSWP-2: Multimodel analysis and implications for our perception of the land surface, *Bull. Am. Meteorol. Soc.*, **87**, 1397–1831.

Entin, K. K., A. Robock, K. Y. Vinnikov, V. Zabelin, S. Liu, and A. Namkhai (1999), Evaluation of Global Soil Wetness Project soil moisture simulations, *J. Meteorol. Soc. Jpn.*, **77**, 183–198.

Falge, E., et al. (2005), *FLUXNET Marconi Conference Gap-Filled Flux and Meteorology Data, 1992–2000*, Available at <http://www.daac.ornl.gov>, Oak Ridge National Laboratory Distributed Active Archive Center, Oak Ridge, Tenn.

Foresee, F. D., and M. T. Hagan (1997), Gauss-Newton approximation to Bayesian regularization, paper presented at IEEE 1997 International Joint Conference on Neural Networks (IJCNN '97), IEEE, Houston, Tex., June 1997.

- Francis, R., et al. (1991), The ERS-1 spacecraft and its payload, *ESA Bull.*, 65, 27–48.
- Franks, S. W., and K. J. Beven (1997), Bayesian estimation of uncertainty in land surface-atmosphere flux predictions, *J. Geophys. Res.*, 102(D20), 23,991–23,999.
- Franks, S. W., K. J. Beven, and J. C. H. Gash (1999), Multi-objective conditioning of a simple SVAT model, *Hydrol. Earth Syst. Sci.*, 34(4), 477–489.
- Frison, P. L., and E. Mougin (1996), Monitoring global vegetation dynamics with ERS-1 wind scatterometer data, *Int. Remote Sens. J.*, 17, 3201–3218.
- Guo, Z., and P. A. Dirmeyer (2006), Evaluation of the second Global Soil Wetness Project soil moisture simulations. 1: Intermodel comparison, *J. Geophys. Res.*, 111, D22S02, doi:10.1029/2006JD007233.
- Gupta, H. V., S. Sorooshian, and P. O. Yapo (1998), Toward improved calibration of hydrologic models: Multiple and noncommensurable measures of information, *Water Resour. Res.*, 34(4), 751–763.
- Gupta, H. V., L. A. Bastidas, S. Sorooshian, W. J. Shuttleworth, and Z. L. Yang (1999), Parameter estimation of a land surface scheme using multi-criteria methods, *J. Geophys. Res.*, 104(D16), 19,941–19,503.
- Gutman, G. G. (1999), On the use of long-term global data of land reflectances and vegetation indices from the advanced very high resolution radiometer, *J. Geophys. Res.*, 104, 6241–6255.
- Hall, F., E. B. de Colstoun, G. Collatz, D. Landis, P. Dirmeyer, A. Betts, G. Huffman, L. Bounoua, and B. Meeson (2006), ISLSCP Initiative II global data sets: Surface boundary conditions and atmospheric forcings for land-atmosphere studies, *J. Geophys. Res.*, 111, D22S01 doi:10.1029/2006JD007366.
- Henderson-Sellers, A., A. Pitman, P. Love, P. Irannejad, and T. Chen (1995), The project for Intercomparison of Land Surface parameterization Schemes (PILPS): Phase 2 and 3, *Bull. Am. Meteorol. Soc.*, 76, 489–503.
- Hollinger, J., R. Lo, G. Poe, R. Savage, and J. Pierce (1987), Special Sensor Microwave/Imager user guide, *Tech. Rep.*, Nav. Res. Lab., Washington, D. C.
- James, M., and S. V. Kalluri (1994), The Pathfinder AVHRR land data set: An improved coarse resolution data set for terrestrial monitoring, *Int. Remote Sens. J.*, 15, 3347–3364.
- Kalnay, E., et al. (1996), The NCEP/NCAR 40-year reanalysis project, *Bull. Am. Meteorol. Soc.*, 77, 437–471.
- Krasnopolski, V. (2007), Neural network emulations for complex multi-dimensional geophysical mappings: Applications of neural network techniques to atmospheric and oceanic satellite retrievals and numerical modeling, *Rev. Geophys.*, 45, RG3009, doi:10.1029/2006RG000200.
- Krinner, G., N. Viovy, N. de Noblet, J. Ogée, P. Friedlingstein, P. Ciais, S. Sitch, J. Polcher, and I. Prentice (2005), A dynamic global vegetation model for studies of the coupled atmosphere-biosphere system, *Global Biogeochem. Cycles*, 19, GB1015, doi:10.1029/2003GB002199.
- Kustas, W., and K. Humes (1997), Spatially distributed sensible heat flux over a semi-arid watershed. Part II: Use of radiometric surface temperatures and a spatially uniform resistance, *J. Appl. Meteorol.*, 36(4), 293–301.
- Kustas, W., and J. Norman (2000), A two-source energy balance approach using directional radiometric temperature observations for sparse canopy covered surfaces, *Agron. J.*, 92, 847–854.
- Law, B., et al. (2002), Environmental controls over carbon dioxide and water vapor exchange of terrestrial vegetation, *Agric. For. Meteorol.*, 113, 97–120.
- Magagi, R., and Y. Kerr (1997), Retrieval of soil moisture and vegetation characteristics by use of ERS-1 wind scatterometer over arid and semi-arid areas, *J. Hydrol.*, 188–189, 361–384.
- Mahrt, L., and K. Ek (1984), The influence of atmospheric stability on potential evaporation, *J. Clim. Appl. Meteorol.*, 23, 222–234.
- Mahrt, L., and H. Pan (1984), A two-layer model of soil hydrology, *Boundary Layer Meteorol.*, 29(1–20).
- Massman, W., and X. Lee (2002), Eddy covariance flux corrections and uncertainties in long-term studies of carbon and energy exchanges, *Agric. For. Meteorol.*, 113, 121–144.
- Mecikalski, J., G. Diak, M. Anderson, and J. Norman (1999), Estimating fluxes on continental scales using remotely sensed data in an atmospheric land exchange model, *J. Appl. Meteorol.*, 38, 1352–1369.
- Meng, C., R. Pinker, J. Tarpley, and I. Laszlo (2003), A satellite approach for estimating regional land surface energy, *J. Geophys. Res.*, 108(D22), 8861, doi:10.1029/2002JD003088.
- Moulin, S., L. Kergoat, N. Viovy, and G. Dedieu (1997), Global-scale assessment of vegetation phenology using NOAA/AVHRR satellite, *J. Clim.*, 10, 1154–1170.
- Nguyen, D., and B. Widrow (1990), Improving the learning speed of 2-layer neural networks by choosing initial values of the adaptive weights, paper presented at IEEE 1990 International Joint Conference on Neural Networks (IJCNN '90), IEEE, San Diego, Calif., June 1990.
- Nishida, K., R. Nemani, S. Running, and J. Glassy (2003), An operational remote sensing algorithm of land surface evaporation, *J. Geophys. Res.*, 108(D9), 4270, doi:10.1029/2002JD002062.
- Noilhan, J., and J. Mahfouf (1996), The ISBA land surface parameterization scheme, *Global Planet. Change*, 13, 145–159.
- Norman, J., W. Kustas, and K. Humes (1995), A two-source approach for estimating soil and vegetation energy fluxes from observations of directional radiometric surface temperature, *Agric. For. Meteorol.*, 77, 263–293.
- Pan, H., and L. Mahrt (1987), Interaction between soil hydrology and boundary-layer development, *Boundary Layer Meteorol.*, 38, 185–202.
- Prigent, C., W. B. Rossow, and E. Mathews (1997), Microwave land surface emissivities estimated from SSM/I observations, *J. Geophys. Res.*, 102(D18), 21,867–21,890.
- Prigent, C., F. Aires, W. Rossow, and E. Matthews (2001a), Joint characterization of vegetation by satellite observations from visible to microwave wavelength: A sensitivity analysis, *J. Geophys. Res.*, 106, 20,665–20,685.
- Prigent, C., F. Aires, W. Rossow, and E. Matthews (2001b), Joint characterization of vegetation by satellite observations from visible to microwave wavelength: A sensitivity analysis, *J. Geophys. Res.*, 106(D18), 20,665–20,685.
- Prigent, C., F. Aires, W. Rossow, and A. Robock (2005), Sensitivity of satellite microwave and infrared observations to soil moisture at a global scale: Relationship of satellite observations to in situ soil moisture measurements, *J. Geophys. Res.*, 110, D07110, doi:10.1029/2004JD005087.
- Prigent, C., F. Aires, and W. Rossow (2006), Land surface microwave emissivities over the globe for a decade, *Bull. Am. Meteorol. Soc.*, 87, 1573–1584.
- Rodell, M., et al. (2004), The Global Land Data Assimilation System, *Bull. Am. Meteorol. Soc.*, 85, 381–394.
- Rossow, W., and R. Schiffer (1999), Advances in understanding clouds from ISCCP, *Bull. Am. Meteorol. Soc.*, 80(11), 2261–2287.
- Schmullius, C. (1997), Monitoring Siberian forests and agriculture with the ERS-1 wind scatterometer, *IEEE Trans. Geosci. Remote Sens.*, 35, 1363–1366.
- Sellers, P., et al. (1997), BOREAS in 1997: Experiment overview, scientific results, and future directions, *J. Geophys. Res.*, 102(D24), 28,731–28,769.
- Stackhouse, P., S. Gupta, S. Cox, J. Mikovitz, T. Zhang, and M. Chiacchio (2004), 12-Year surface radiation budget data set, *GEWEX News*, 14(4), 10–12.
- Tarpley, J. (1994), Monthly evapotranspiration from satellite and conventional meteorological observations, *J. Clim.*, 7(5), 704–713.
- Viterbo, P., and A. Beljaars (1995), An improved land surface parameterization scheme in the ECMWF model and its validation, *J. Clim.*, 8, 2716–2748.
- Wagner, W., G. Lemoine, and H. Rott (1999), A method for estimating soil moisture from ERS scatterometer and soil data, *Remote Sens. Environ.*, 70, 191–207.
- Wang, K., P. Wang, Z. Li, M. Cribb, and M. Sparrow (2007), A simple method to estimate actual evapotranspiration from a combination of net radiation, vegetation index, and temperature, *J. Geophys. Res.*, 112, D15107, doi:10.1029/2006JD008351.
- Wilson, K., et al. (2002), Energy partitioning between latent and sensible heat flux during the warm season at FLUXNET sites, *Water Resour. Res.*, 38(12), 1294, doi:10.1029/2001WR000989.
- Wright, I., A. Manzi, and H. da Rocha (1995), Surface conductance of Amazonian pasture: model application and calibration for canopy climate, *Agric. For. Meteorol.*, 75, 51–70.
- Zhang, Y., W. Rossow, A. Lacis, V. Oinas, and M. Mishchenko (2004), Calculation of radiative fluxes from the surface to top of atmosphere based on ISCCP and other global data sets: Refinements of the radiative transfer model and the input data, *J. Geophys. Res.*, 109, D19015, doi:10.1029/2003JD004457.
- Zhang, T., J. Wen, Z. Su, R. van der Velde, J. Timmermans, R. Liu, Y. Liu, and Z. Li (2008), Soil moisture mapping over the Chinese Loess Plateau using ENVISAT/ASAR data, *J. Adv. Space Res.*, 43(7), 1111–1117. doi:10.1016/j.asr.2008.10.030.
- Zhao, M., and P. Dirmeyer (2003), Production and Analysis of GSWP-2 Near-Surface Meteorology Data Sets, *Tech. Rep.*, Center for Ocean-Land-Atmospheric Studies, COLA Technical Report 159.

F. Aires, Laboratoire de Météorologie Dynamique, Institut Pierre-Simon Laplace/Centre National de la Recherche Scientifique, Université Pierre et Marie Curie, case 99, 4, Place Jussieu, F-75252 Paris, France.

C. Jiménez and C. Prigent, Laboratoire d'Études du Rayonnement et de la Matière en Astrophysique, Centre National de la Recherche Scientifique, Observatoire de Paris, 61, Avenue de l'Observatoire, F-75014 Paris, France. (carlos.jimenez@obspm.fr)